

*W. W. Wainman
The Editor*
Mullard Technical Communications

Splitbeam

VOLUME 7 NUMBER 67 December 1963



Mullard Technical Communications

VOLUME 7 NUMBER 67 December 1963

Contents	Transistor Decoder Circuits for F.M. Stereo Broadcasting <i>G. D. Browne</i>	202
	Capacitive Intermodulation in Dual-trace Oscilloscope Tubes <i>D. Styles</i>	206
	Timebases for Sampling Oscilloscopes <i>B. Gilbert</i>	211
	Microphony in Tape Recorders <i>S. S. Dagpunar</i>	227

Mullard Technical Communications contains information on the performance or application of Mullard products such as electronic valves and tubes, semiconductor devices, and electrical and magnetic components. It is issued free-of-charge to equipment designers, research organisations, reference libraries, and educational establishments. Bona fide applications to be added to the circulation list should be made under an official letter head to the Technical Information Department. Overseas enquiries should be addressed to the local Mullard agent, or to Mullard Overseas Ltd. at Mullard House.

Abstracts, or references to an article, should mention both the source, *Mullard Technical Communications*, and the authors. Requests for republication or translation should be made to the Editor in writing.

The issue of the information contained in this publication does not imply any authority or licence for the utilisation of any patented feature.

'Mullard' is the trade mark of Mullard Limited and is registered in most of the principal countries of the world.

Editor: F. A. Sowan

Assistant Editors: E. G. Evans R. Barrie

Published by

Technical Information Department
Mullard Limited, Mullard House, Torrington Place, London, W.C.1
LANgham 6633

© Mullard Limited, 1963

Made and Printed in England by

WIGHTMAN AND COMPANY LIMITED, 1/3 BRIXTON ROAD, LONDON, S.W.9

Transistor Decoder Circuits for F.M. Stereo Broadcasting

G. D. BROWNE

Mullard Research Laboratories

This article describes two transistor decoders for use with the F.C.C. approved (G.E.-Zenith) v.h.f. f.m. stereophonic broadcasting system.

One circuit employs two transistors, two semiconductor diodes, and is for use with valve circuits. The other retains the basic simplicity of the first circuit, but uses four transistors and operates by means of a switching process. It is suitable for valve or transistor circuits and provides inherent reverse compatibility.

A stereo indicator ('beacon') circuit is also described.

INTRODUCTION

Two simple valve-equipped decoders have already been described (Ref. 1). The present article describes the transistor counterparts of the valve-equipped decoders. A full discussion on transistor decoder circuits can be found in Ref. 2.

An attempt has been made to design:

- (i) A simple transistor decoder for use with valve-equipped ratio detectors and audio amplifiers, and
- (ii) A versatile decoder to operate from all normal ratio detectors, either valve or transistor, and to feed into any conventional amplifiers (valve or transistor).

The first decoder circuit (Fig. 1) is of particular use where it is difficult or impossible to obtain h.t. and l.t. supplies for a valve decoder. This difficulty is likely with a.c./d.c. equipment. The necessary power supply for a transistor decoder may readily be obtained from the cathode circuit of an output valve or by rectifying the heater voltage of the valve at the earthy end of the chain.

The second circuit (Fig. 3) will fulfil the same functions as the first decoder circuit but it has the added advantage that its output impedance is sufficiently low to drive a transistor audio amplifier. This circuit also provides inherent reverse compatibility.

To meet any demand for a visual indication that a stereo broadcast is in progress, a two-transistor circuit is described. This design is capable of switching on a 1.2W low-voltage lamp (Fig. 7).

SIMPLE TWO-TRANSISTOR DECODER

The circuit of the two-transistor decoder is shown in Fig. 1. It is designed primarily to operate from a valve ratio detector and is suitable only for valve-equipped audio amplifiers with high input impedances.

To achieve an overall gain of approximately unity, the complete multiplex signal is first amplified by an OC81

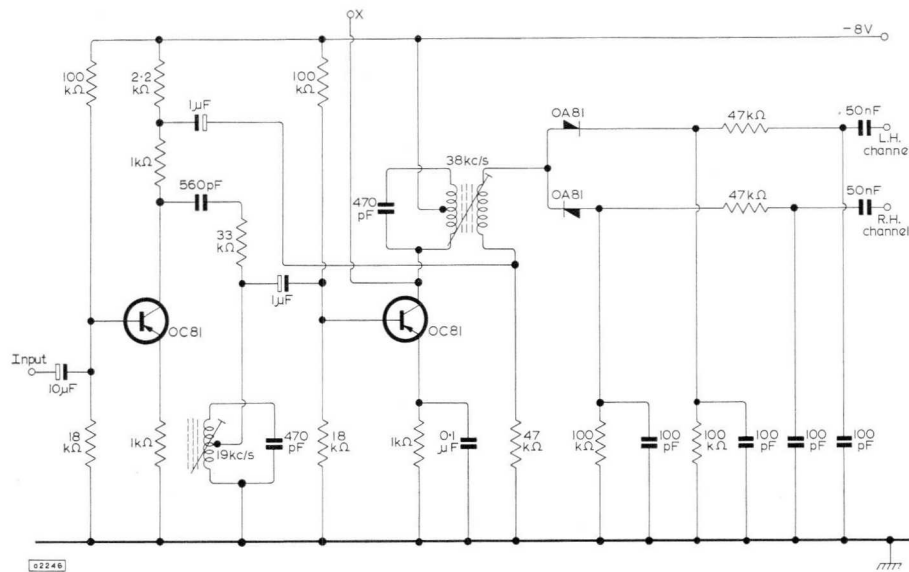
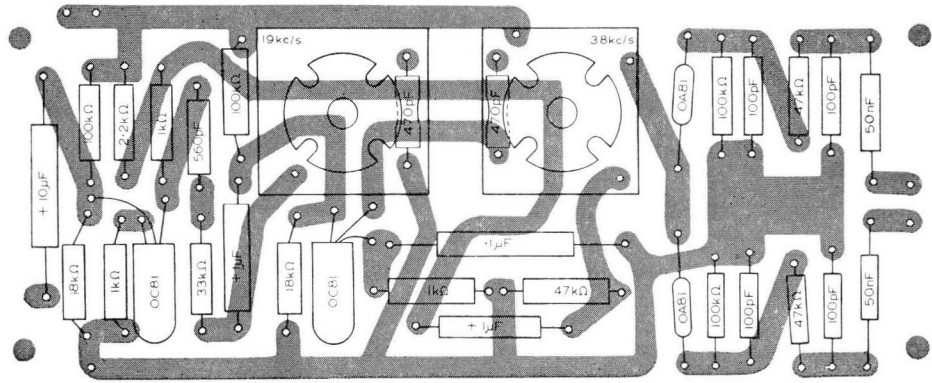
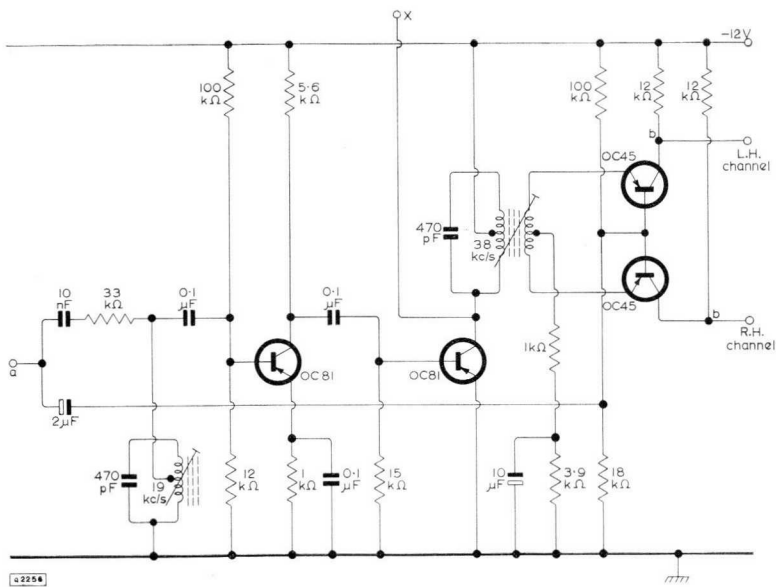


Fig. 1—Simple two-transistor decoder

Fig. 2—
Suggested printed
board layout for
simple decoder



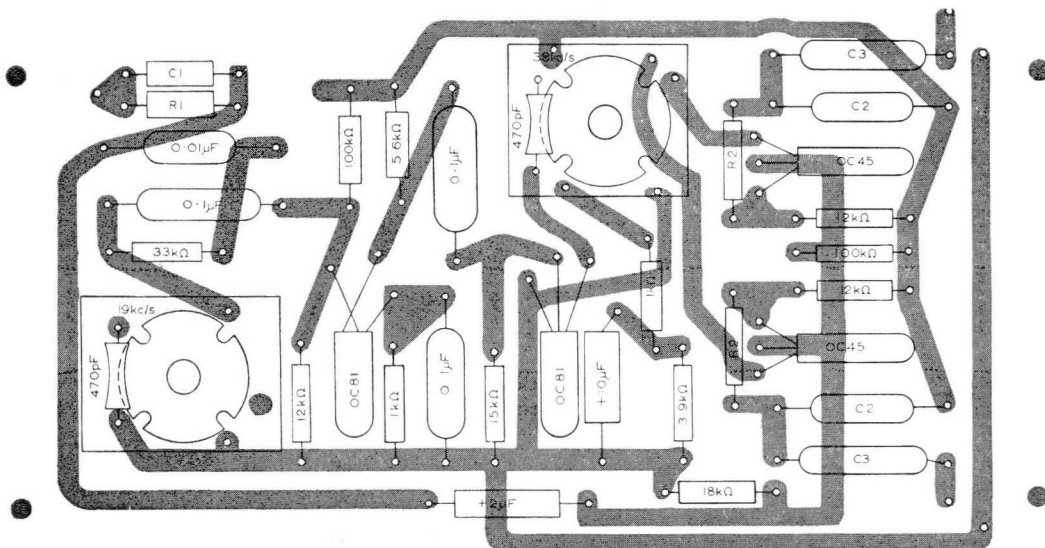
2254



2254

Fig. 3—
Four-transistor
decoder

Fig. 4—
Suggested printed
board
layout for
four-transistor
decoder



2255

operating with heavy feedback, thereby providing a relatively high input impedance and adequate freedom from distortion. The entire output is fed by way of a

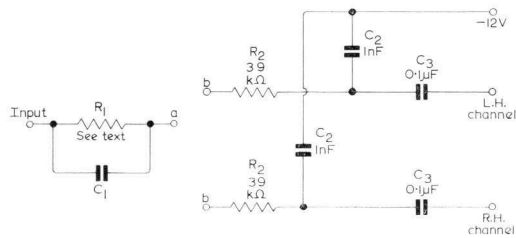


Fig. 5—Valve input and output circuits

picofarads). Such an arrangement not only provides the correct input level at all multiplex frequencies but also reduces discriminator loading to an acceptable value.

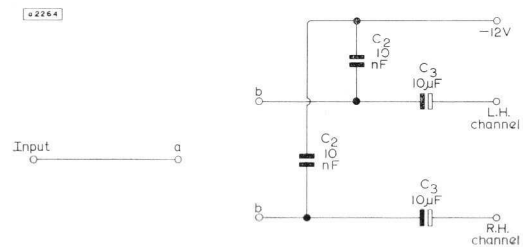


Fig. 6—Transistor input and output circuits

phase correcting network to the 19kc/s circuit which extracts the pilot sub-carrier. Frequency doubling occurs in the second OC81, to produce a 38kc/s signal across the tuned primary of the transformer in the collector circuit. The requisite fraction of the amplified multiplex signal is connected to one end of the 38kc/s transformer secondary winding. Demodulation of the sidebands and matrixing occur in the diode circuits in the usual way.

Reverse compatibility is not inherent with this arrangement but can be readily achieved by the simple expedient of connecting the two outputs together, preferably immediately following the diodes themselves. This technique preserves the best possible signal-to-noise ratio for monophony.

The decoder will handle signals of up to 1.5V peak-to-peak at its input (corresponding to a discriminator e.m.f. of approximately 3V peak-to-peak) with a power supply of 8V at 2mA, or approximately 2.75V with a supply voltage of 12V at 3mA. The measured cross-talk is better than -20dB. A suggested layout for this decoder is shown in Fig. 2.

FOUR-TRANSISTOR DECODER

A more flexible and versatile decoder is illustrated in Fig. 3 operating with a 12V, 2.5mA supply.

The pilot sub-carrier is extracted immediately following the discriminator output by means of a 19kc/s tuned circuit. The sub-carrier is subsequently amplified by an OC81 transistor. Frequency doubling occurs in the second OC81 to produce a 38kc/s signal in the transformer primary winding, which is situated in the collector circuit of the second OC81. A centre-tapped secondary winding supplies anti-phase switching signals to the emitters of two OC45 transistors, and the complete multiplex information is applied to their bases, which are directly coupled. The separate stereo outputs thus appear across the 12kΩ collector loads.

The input impedance of the decoder is approximately 15kΩ and the decoder may be fed directly from a transistor discriminator, capable of providing a loaded output of some 750mV peak-to-peak. It may also be fed from a typical valve discriminator, in which case it is convenient to attenuate the discriminator output by means of a series resistance (typically between 3.3kΩ and 33kΩ) shunted by a suitable capacitor (generally a few hundred

The output circuits are of approximately 12kΩ impedance. The output may therefore be taken by way of normal de-emphasis networks to conventional valve audio amplifiers. The de-emphasis capacitors can be placed directly across the decoder output loads, for connection to transistor amplifiers. Circuit details for the various input and output conditions are shown in Figs. 5 and 6.

Reverse compatibility is inherent in this decoder circuit, since the OC45 transistors operate under class A conditions in the absence of a 19kc/s pilot sub-carrier. Normal monophonic output is therefore available with the best possible signal-to-noise ratio.

With typical valve circuits connected to the input and output stages, the decoder gives a gain of some 10dB under stereo conditions and approximately the same with monophonic signals. If required, the gain values can be modified by changing the value of the OC45 collector load resistors. The measured cross-talk is better than -20dB.

With the use of fully transistorised equipment the stereo gain is in excess of unity under typical working conditions.

A suggested printed wiring board layout for this decoder is shown in Fig. 4.

STEREO INDICATOR

There may be a demand for an indication that a stereo broadcast is taking place. For this reason a circuit employing a simple two-transistor visual indicator is described (Fig. 7).

An obvious feature of a stereophonic broadcasting system is the 19kc/s sub-carrier. In a decoder employing normal frequency doubling, the regenerated 38kc/s signal can be utilised. Since the 38kc/s signal voltage is of considerably greater amplitude than the 19kc/s signal, it is easier to recognise its presence. A typical circuit arrangement is shown in Fig. 7.

An output at 38kc/s is extracted at a point 'X' from either of the circuits shown in Fig. 1 or 3. This output is fed through a limiting resistor and isolating capacitor to an OC81 transistor connected in the emitter-follower configuration. The output from the OC81 is directly connected to the base of a second OC81. The second OC81 thus conducts with the result that the small lamp

in its collector circuit glows. In the absence of the 19kc/s sub-carrier and thus the 38kc/s output, the second transistor is cut off and the lamp is extinguished.

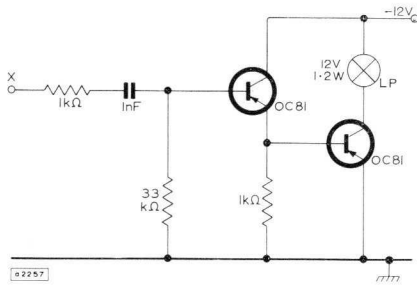


Fig. 7—Stereo indicator circuit

PERFORMANCE

The two decoders described were tested in conjunction with a variety of ratio detectors and their outputs were coupled to typical audio amplifiers. The results obtained indicate that the two circuits described are more than adequate for normal domestic purposes with measured cross-talk considerably better than -20dB.

Both decoders and the indicator circuit accept normal spreads in the transistor types used.

COIL DETAILS

Mullard Vinkor pot cores type LA2505 were used in the decoders described.

19kc/s coil (Fig. 1)	140mH
990 turns	43 s.w.g. enamelled copper wire tapped at 135 turns from the earthy end, tuned with 470pF ± 2%. Mullard type WF2948
19kc/s coil (Fig. 3)	140mH
990 turns	43 s.w.g. enamelled copper wire tapped at 40 turns from the earthy end, tuned with 470pF ± 2%. Mullard type WF2949
38kc/s transformer (Fig. 1)	
Secondary (wound first)	36 s.w.g. enamelled copper wire
120 turns	
Primary 35mH	43 s.w.g. enamelled copper wire, tapped at 60 turns from the start (collector end), tuned with 470pF ± 2%. Mullard type WF2950
495 turns	
38kc/s transformer (Fig. 3)	
Primary 35mH	39 s.w.g. enamelled copper wire tapped at 60 turns from the start (collector end), tuned with 470pF ± 2%. Mullard type WF2951
495 turns	
Secondary	39 s.w.g. enamelled copper wire centre tapped
12 turns	

REFERENCES

1. BROWNE, G. D. 'Simple Decoders (Adaptors) for use with the F.C.C. Stereo VHF Broadcasting System'. **Mullard Technical Communications**, Vol. 6, No. 59, August 1962, pp. 360 to 367.
2. BROWNE, G. D. 'Transistorised Decoders for FM Stereo'. **Hi-Fi News**, Vol. 8, No. 1, June 1963, pp. 38 to 44.

Capacitive Intermodulation in Dual-trace Oscilloscope Tubes

D. STYLES

Mullard Applications Research Laboratory

In any c.r.t. with two or more electrostatic deflection systems, some degree of capacitive intermodulation between the systems may be encountered. This article shows the manner in which interaction is affected by (a) the direct capacitances (b) variations in frequency and (c) the external circuit. A split beam tube has been examined for the purpose of the calculations but the reasoning is equally applicable to double-gun systems and to x-to-y intermodulation.

INTRODUCTION

If a c.r.t. has two or more electrostatic deflection systems there may exist some form of intermodulation between the systems. This can occur in two basic forms, namely field intermodulation and capacitive intermodulation. Field intermodulation results directly from the effect of the electrostatic field, due to one set of deflector plates, upon the beam passing through the other system. The effect in any one system will be constant at all frequencies from d.c. upwards. Capacitive intermodulation is caused by signals induced at the deflector plates of one system, from the deflector plates of the other system, through capacitive coupling. It is the second of these causes, capacitive intermodulation, which is considered in this article. Although this article is based on the considerations for a split-beam tube the intermodulation effect will be present in double-gun tubes in a similar manner.

Other possible reasons for intermodulation are mutual inductance between leads within the tube, and couplings between leads, either capacitive or inductive, external to the tube. Inductive coupling within the tube and in well-constructed circuitry will almost invariably be negligible. Capacitive coupling external to the tube depends upon circuit layout and should be negligible, but otherwise can be dealt with directly as an increase in the cross-coupling capacitances.

In the early days of dual-trace oscillography the split beam tube was the only type of tube available: the double-gun was considered to present too many technical problems.

In the first split-beam tubes the y deflection system consisted of three plates as shown in Fig. 1a. The central plate was connected to a_3 and acted as a shield between the two beams. The outer plates, one on either side, acted as the deflector plates. Each beam was, then, asymmetrically deflected. With this arrangement the capacitive intermodulation between the beams could be ascertained from the capacitance between the two

deflector plates and the capacitances from each deflector plate to earth. For the purpose of published data, the significant value was $c_{(y'-y'')}$ which can be seen from Fig. 1b.

In recent years, double-gun tubes have come into common use and, more recently, symmetrically deflected split beam tubes have been developed. The system of expressing intermodulation capacitance was unfortunately carried over from the old asymmetric tubes and published data

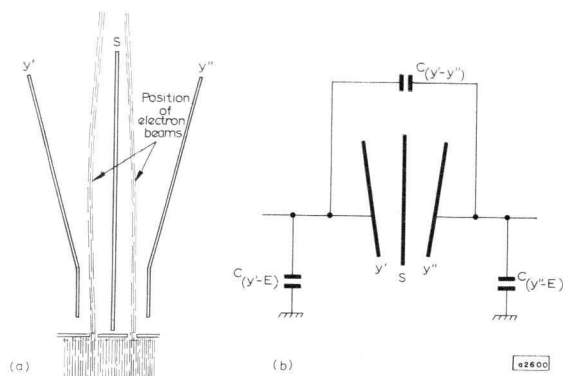


Fig. 1—Simplified structure of asymmetric split-beam deflection system, and the associated capacitances

often shows the capacitance $c_{(y1'+y2')-(y1''+y2'')}$. This capacitance has only limited practical significance and it is the purpose of this article to show the manner in which capacitive intermodulation is related to inter-electrode capacitances.

While the calculations that follow are intended to apply to the dual trace tubes, they are equally applicable to capacitive intermodulation between x and y systems.

CAPACITANCE RELATIONSHIPS

In assessing capacitive intermodulation accurately there are seven admittances directly responsible for interaction which must be taken into account, namely:

- (1) $Y_{(y1'-y1'')}$
- (2) $Y_{(y1'-y2'')}$
- (3) $Y_{(y2'-y1'')}$
- (4) $Y_{(y2'-y2'')}$
- (5) $Y_{(y1''-y2'')}$
- (6) $Y_{(y1''-e)}$
- (7) $Y_{(y2''-e)}$

The suffix numbers define the plate within each system,

the primes define the system (or gun), and e indicates earth. Of these admittances, the first five are purely capacitive. The last two, however, include the output conductance of the scan output valves, and because of this it is simpler for the moment to consider each case as an admittance. The appropriate capacitances and admittances are shown in Fig. 2.

For the purposes of these calculations, the intermodulation voltage (V_{eff}) at the second system ($y_1''y_2''$) is derived in terms of the signal voltage (V_0) applied to the first system ($y_1'y_2'$).

The equivalent circuit involving the seven admittances is shown in Fig. 3 where

- $A = Y_{(y_1' - y_1'')}$
 - $B = Y_{(y_2' - y_1'')}$
 - $C = Y_{(y_1' - y_2'')}$
 - $D = Y_{(y_2' - y_2'')}$
 - $E = Y_{(y_1' - e)}$
 - $F = Y_{(y_2' - e)}$
 - $G = Y_{(y_1'' - y_2'')}$
- Direct intermodulating capacitances
 Plate-to-earth capacitances (including external capacitances)
 Plate-to-plate capacitance

The instantaneous currents through these admittances

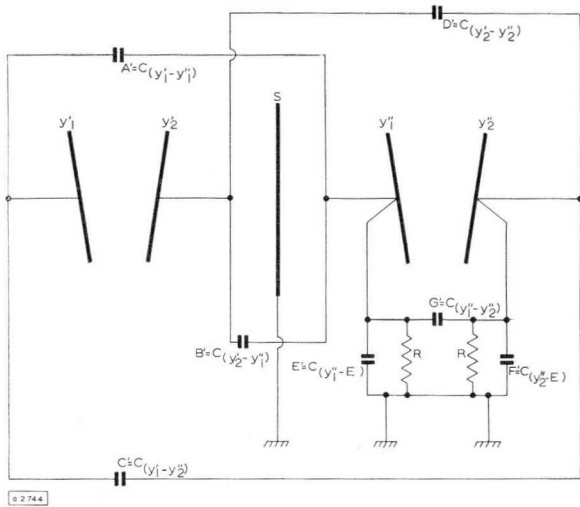


Fig. 2—Capacitances and conductances associated with the symmetrical deflection system. The resistor R represents the output resistance of the driving-stage, and is used in the calculation as the conductance g_a where $g_a = 1/R$

are defined by the corresponding small letters, a, b, c, d, e, f, and g respectively.

Applying Kirchoff's laws the following relationships are established:

- $a + g = e + b$... (1)
- $c + f = g + d$... (2)
- $Ff + Ee + Gg = 0$... (3)
- $V_1 = Aa + Ee$... (4)
- $V_2 = Bb - Ee$... (5)
- $Aa = Cc + Gg$... (6)
- $V_2 = Ff + Dd$... (7)

From Eq (4)

$$a = \frac{V_1 - Ee}{A} \quad \dots(8)$$

From Eq (5)

$$b = \frac{V_2 + Ee}{B} \quad \dots(9)$$

From Eqs (1), (8) and (9)

$$\frac{V_1 - Ee}{A} + g = e + \frac{V_2 + Ee}{B} \quad \dots(10)$$

From Eq (7)

$$d = \frac{V_2 - Ff}{D} \quad \dots(11)$$

From Eqs (11) and (3)

$$d = \frac{V_2 + Ee + Gg}{D} \quad \dots(12)$$

From Eq (6)

$$c = \frac{Aa - Gg}{C} \quad \dots(13)$$

From Eqs (13) and (4)

$$c = \frac{V_1 - Ee - Gg}{C} \quad \dots(14)$$

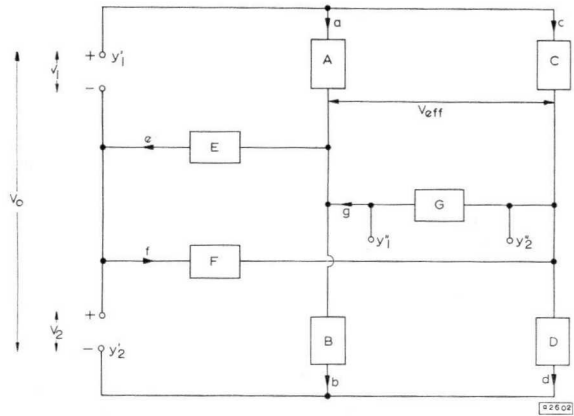


Fig. 3—Equivalent circuit of plate system; the admittances are defined in the text

From Eqs (2), (12) and (14)

$$\frac{V_2 - Ff}{D} + g = f + \frac{V_1 - Ee - Gg}{C} \quad \dots(15)$$

From Eq (3)

$$Ff = -(Ee + Gg) \quad \dots(16)$$

and

$$f = \frac{-(Ee + Gg)}{F} \quad \dots(17)$$

From Eqs (15), (16) and (17)

$$\frac{V_2 + Ee + Gg}{D} + g = \frac{V_1 - Ee - Gg}{C} - \frac{Ee + Gg}{F} \quad \dots(18)$$

which may be rearranged in the form:

$$Ee + Gg = \frac{\frac{V_1}{C} - \frac{V_2}{D} - g}{\left(\frac{1}{D} + \frac{1}{C} + \frac{1}{F}\right)} \quad \dots(19)$$

Eq (10) may be re-written to give:

$$\frac{V_1 - Ee}{A} + g = \frac{Ee}{E} + \frac{V_2 + Ee}{B} \quad \dots(20)$$

This may now be rearranged to give:

$$E_e = \frac{\frac{V_1}{A} - \frac{V_2}{B} + g}{\left(\frac{1}{A} + \frac{1}{B} + \frac{1}{E}\right)} \dots (21)$$

Subtracting Eq (21) from Eq (19)

$$G_g = \frac{\frac{V_1}{C} - \frac{V_2}{D} - g}{\left(\frac{1}{C} + \frac{1}{D} + \frac{1}{F}\right)} - \frac{\frac{V_1}{A} - \frac{V_2}{B} + g}{\left(\frac{1}{A} + \frac{1}{B} + \frac{1}{E}\right)} \dots (22)$$

This expression is somewhat simplified if we consider the case of balanced symmetrical input to the $y_{1'}$ $y_{2'}$ plates. Referring to Fig. 3 we can now consider that $V_1 = V_2 = V_o/2$ where V_o is the voltage applied between $y_{1'}$ and $y_{2'}$. Hence,

$$G_g = \frac{\frac{V_o}{2}\left(\frac{1}{C} - \frac{1}{D}\right) - g}{\left(\frac{1}{C} + \frac{1}{D} + \frac{1}{F}\right)} - \frac{\frac{V_o}{2}\left(\frac{1}{A} - \frac{1}{B}\right) + g}{\left(\frac{1}{A} + \frac{1}{B} + \frac{1}{E}\right)} \dots (23)$$

Replacing $\left(\frac{1}{C} + \frac{1}{D} + \frac{1}{F}\right)$ with X and $\left(\frac{1}{A} + \frac{1}{B} + \frac{1}{E}\right)$ with Z, gives

$$G_g X Z = \frac{V_o}{2}\left(\frac{1}{C} - \frac{1}{D}\right)Z - \frac{G_g}{G}Z - \frac{V_o}{2}\left(\frac{1}{A} - \frac{1}{B}\right)X - \frac{G_g}{G}X \dots (24)$$

Rearrangement of Eq (24) gives

$$G_g \left(XZ + \frac{Z}{G} + \frac{X}{G} \right) = \frac{V_o}{2} \left[\left(\frac{1}{C} - \frac{1}{D} \right) Z - \left(\frac{1}{A} - \frac{1}{B} \right) X \right]$$

Therefore

$$\frac{G_g}{V_o} = \frac{\frac{Z}{2} \left(\frac{1}{C} - \frac{1}{D} \right) - \frac{X}{2} \left(\frac{1}{A} - \frac{1}{B} \right)}{XZ + \frac{X+Z}{G}} \dots (25)$$

But G_g will be the voltage appearing between the $y_{1'}$ and $y_{2'}$ plates. This is the effective intermodulation voltage and will be denoted as V_{eff} .

Substituting once again for the terms X and Z, the percentage intermodulation between the two deflection systems will be given by Eq (26) on page 209.

The Simplified Case

It is often convenient, and certainly much simpler, to consider the condition where the second set of deflector plates is open-circuited. The conductance due to the driving stages is ignored and all of the admittances become purely capacitive. This represents the worst case of intermodulation obtainable for any given set of capacitances and is a limit figure for the c.r.t.

Each admittance may be replaced by the appropriate value of ωC and since ω appears in the same order in both numerator and denominator the percentage intermodulation, as shown in Eq (26), can be written as in Eq (27) on page 209, where the prime associated with each symbol indicates that it represents the actual value of capacitance (for example $A = 1/j\omega A'$).

The expression may be further simplified if we choose to ignore the term G' which represents the capacitance between the plates of the second system. This in itself could result in an error of the order of 30% in the typical case of the Mullard E10-11GH if tube capacitances only were being considered. However, it must be remembered that in practice the deflection circuit output capacitances will appear in parallel with E' and F' , tending to reduce the error to something much closer to 10%.

Eq (27) will now become

$$\frac{V_{eff}}{V_o} \% = \frac{1}{2} \left[\frac{(C' - D')}{(C' + D' + F')} - \frac{(A' - B')}{(A' + B' + E')} \right] \times 100 \% \dots (28)$$

From this it can be seen that it is not so much the actual values of A' , B' , C' , and D' which are significant, but rather the relationship between them.

A much more reasonable approximation may be derived from the fact that the capacitances A' , B' , C' , and D' are almost invariably small compared with E' and F' and Eq (27) may be reduced to

$$\frac{V_{eff}}{V_o} \% = \frac{1}{2} \left[\frac{E'(C' - D') - F'(A' - B')}{E'F' + G'(E' + F')} \right] \times 100 \% \dots (29)$$

where errors will be of the order of 1 or 2%, which is considerably better than the accuracy to which the smaller capacitances can be measured.

The Practical Case

If we take into account the conductance g_d introduced by the driving valve circuit then the terms $1/E$ and $1/F$ in Eq (26) become $g_d + j\omega E'$ and $g_d + j\omega F'$. Since it has already been assumed that both sets of plates are driven symmetrically, the conductance g_d in both terms will be the same. Eq (26) now becomes Eq (30).

To simplify the units involved, a very close approximation may be made as shown in Eq (31), where f is a specific frequency of interest and f_o is the high frequency 3dB point of the output stage driving the set of plates between which intermodulation is being measured (that is, $f_o = g_d/2\pi E'$). The assumption is made in Eq (31) that the capacitances E' and F' are similar in value, and since these values will include strays and valve output capacitances in a balanced arrangement, this is a reasonable assumption.

Once again, if A' , B' , C' , and D' are small compared with E' and F' , a much more practical expression may be derived as in Eq (32).

It is interesting to note that if E' and F' are in fact identical then a further simplification may be made:

$$\frac{V_{eff}}{V_o} \% = \frac{100}{2} \left[\frac{(C' - D') - (A' - B')}{\left(E' - \frac{jf_o E'}{f} \right) + 2G'} \right] \% \dots (33)$$

Since the values of the capacitances E' and F' determine the bandwidth of the output stage of the amplifier it may be reasonable in some cases to ensure by means of padding-capacitances that these are equal. Thus both sides of the output stage would have the same bandwidth, and the possibility of high frequency distortions would be reduced.

$$\frac{V_{eff}}{V_o} \% = \frac{1}{2} \left[\frac{\left(\frac{1}{A} + \frac{1}{B} + \frac{1}{E}\right)\left(\frac{1}{C} - \frac{1}{D}\right) - \left(\frac{1}{C} + \frac{1}{D} + \frac{1}{F}\right)\left(\frac{1}{A} - \frac{1}{B}\right)}{\left(\frac{1}{A} + \frac{1}{B} + \frac{1}{E}\right)\left(\frac{1}{C} + \frac{1}{D} + \frac{1}{F}\right) + \frac{1}{G}\left(\frac{1}{A} + \frac{1}{B} + \frac{1}{C} + \frac{1}{D} + \frac{1}{E} + \frac{1}{F}\right)} \right] \times 100 \% \dots(26)$$

$$\frac{V_{eff}}{V_o} \% = \frac{1}{2} \left[\frac{(A'+B'+E')(C'-D') - (C'+D'+F')(A'-B')}{(A'+B'+E')(C'+D'+F') + G'(A'+B'+C'+D'+E'+F')} \right] \times 100 \% \dots(27)$$

$$\frac{V_{eff}}{V_o} \% = \frac{100}{2} \left[\frac{\left(A'+B'+E' - \frac{jg_d}{\omega}\right)(C'-D') - \left(C'+D'+F' - \frac{jg_d}{\omega}\right)(A'-B')}{\left(A'+B'+E' - \frac{jg_d}{\omega}\right)\left(C'+D'+F' - \frac{jg_d}{\omega}\right) + G'\left(A'+B'+C'+D'+E'+F' - \frac{2jg_d}{\omega}\right)} \right] \% \dots(30)$$

$$\frac{V_{eff}}{V_o} \% = \frac{100}{2} \left[\frac{\left(A'+B'+E' - \frac{jf_o E'}{f}\right)(C'-D') - \left(C'+D'+F' - \frac{jf_o F'}{f}\right)(A'-B')}{\left(A'+B'+E' - \frac{jf_o E'}{f}\right)\left(C'+D'+F' - \frac{jf_o F'}{f}\right) + G'\left(A'+B'+C'+D'+E'+F' - \frac{jf_o}{f}(E'+F')\right)} \right] \% \dots(31)$$

$$\frac{V_{eff}}{V_o} \% = \frac{100}{2} \left[\frac{\left(E' - \frac{jf_o E'}{f}\right)(C'-D') - \left(F' - \frac{jf_o F'}{f}\right)(A'-B')}{\left(E' - \frac{jf_o E'}{f}\right)\left(F' - \frac{jf_o F'}{f}\right) + G\left(E'+F' - \frac{jf_o}{f}(E'+F')\right)} \right] \% \dots(32)$$

It should be noted, however, that if E' and F' are not very similar and intermodulation is in fact small, then considerable errors may result from the use of Eq (33).

A curve is given in Fig. 4 showing the manner in which intermodulation varies with frequency, or rather with the ratio f/f_o, in the practical case. It should be noted that it is

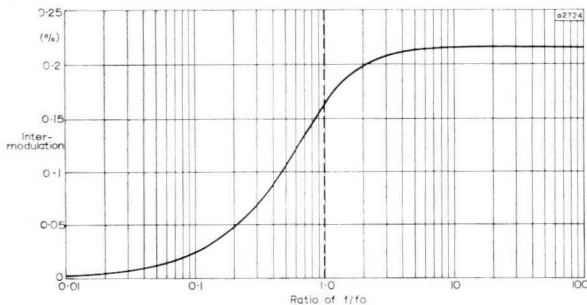


Fig. 4—Intermodulation as a function of frequency

the reciprocal of this ratio which appears in the calculations. It can be seen that at low frequencies the intermodulation tends to zero since the capacitances E' and F' become effectively short-circuited by the output conductance of the driving source. At high frequencies the curve flattens

to a constant value which is that given by the purely capacitive case considered earlier.

If it is considered that both driven plates and the plates receiving cross-modulation are supplied by circuits having the same bandwidth then the vertical dotted line in Fig. 4 indicates the 3dB point where f = f_o. For most practical purposes, this is the highest frequency of interest in any given system.

Reverse Intermodulation

It is of interest at this point to consider the expression for the intermodulation voltage between the y₁-y₂' plates caused by a signal applied to the y₁'-y₂' plates. In the approximate form corresponding to Eq (33) this will be

$$\frac{V_{eff}}{V_o'} \% = \frac{100}{2} \left[\frac{(A'-C') - (B'-D')}{H' - \left(\frac{jf_o H'}{f}\right) + 2K} \right] \% \dots(34)$$

where H' and K' are the capacitances c_(y1'-e) or c_(y2'-e), and c_(y1'-y2') respectively. From Eqs (33) and (34) it may be stated that, if (A'+D') = (B'+C') then intermodulation in both directions will be zero; that is, there will be no modulation in either trace. This relies on the assumption which led to the simplification of the expression, namely that E' = F'. If E' is not equal to F' then intermodulation will be zero in both directions only when A' = B' = C' = D'.

Example

A typical practical case has been worked and is illustrated by curve A in Fig. 5. The capacitance values used were:

A'	0.03pF	E'	3.0pF
B'	0.05pF	F'	3.0pF
C'	0.01pF	G'	0.6pF
D'	0.02pF		

The curve A illustrates the behaviour of the intermodulation as the external capacitance between each plate and earth is increased from zero to 12pF. This curve

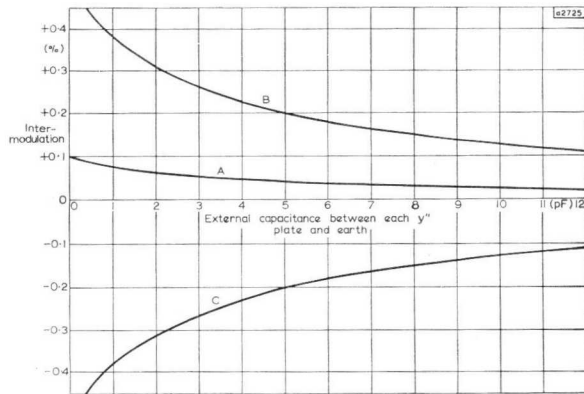


Fig. 5—The effect of external y-plate capacitance on intermodulation

shows the general behaviour rather than absolute values of intermodulation. It has therefore been calculated in the simple form from Eq (33), for the 3dB point, that is, where $f = f_0$.

Since the capacitances A', B', C', and D' are the significant values in the calculation of intermodulation, the limit values of these capacitances must be considered. If the assumption is made that each of these capacitances may vary between zero and 0.05pF, then the worst cases of intermodulation will occur when B' and C' are zero

and A' and D' are at a maximum, or vice versa. These two limit cases are shown by curves B and C. The use of the negative sign in association with the percentage intermodulation indicates phase reversal of the modulation signal relative to the signal causing the intermodulation.

TUBE SPECIFICATION

It has been shown that to define intermodulation with any degree of accuracy it would be necessary to know the actual value of four capacitances for each individual tube, in addition to those normally published. Since each of these capacitances would be subject to normal manufacturing tolerances, which, it has been shown, cause considerable variation in intermodulation, it is not possible to publish a practical general value. If, on the other hand, maximum and minimum values were quoted for each of these four additional capacitances it would still only be possible to define the worst case of intermodulation possible. If we consider the case which would give the worst intermodulation from Eq (33) then (B'+C') will be at a maximum, while (A'+D') are at a minimum, or vice versa. If we now say that the minimum value for any of the capacitances is zero it would make no difference if we wrote the numerator as A'+B'+C'+D' since either A' and D', or B' and C', are now zero. The generally published value $C_{(y1'+y2')-(y1''+y2'')}$ is in fact identical to A'+B'+C'+D'.

Therefore it can be said that if the published value of $C_{(y1'+y2')-(y1''+y2'')}$ is suitably low, then intermodulation will be satisfactory. A high value of published capacitance does not, however, signify a large degree of intermodulation.

Therefore, in recent published data the maximum magnitude of intermodulation signal appearing at the screen for a given applied signal amplitude is quoted for the condition where the modulated plates are effectively open-circuited. For most users this is the most convenient way of presenting information on intermodulation. For special applications it can be seen from the article that zero intermodulation may be obtained by suitably trimming the appropriate capacitances.

Timebases for Sampling Oscilloscopes

B. GILBERT

Mullard Semiconductor Measurement and Application Laboratory

Trigger, timebase and scanning circuits for a sampling oscilloscope are described in this article. The effective time scale achieved is down to 0.5ns/cm.

INTRODUCTION

This article describes the trigger, timebase and scanning circuits of a practical sampling oscilloscope, developed as a general purpose instrument giving effective time scales down to 0.5ns/cm. The circuits described constitute an inexpensive attachment for use with any existing oscilloscope, but they are also suitable for incorporation into a complete instrument. A later article will describe the signal circuits for sampling.

progression is under the control of a 'staircase generator', which also provides the horizontal deflection voltage for the c.r.t. Each time the staircase generator resets, the delay returns to the minimum value, and the cycle is repeated. These pulses subsequently fire the sampling-pulse (or "strobe-pulse") generator to sample the signal.

The delay variation through each complete cycle of the staircase corresponds to the effective timebase length on the c.r.t. display. The start of the timebase can be delayed by a variable 'trigger' delay to permit the required portion of the displayed waveform to be selected. This delay has

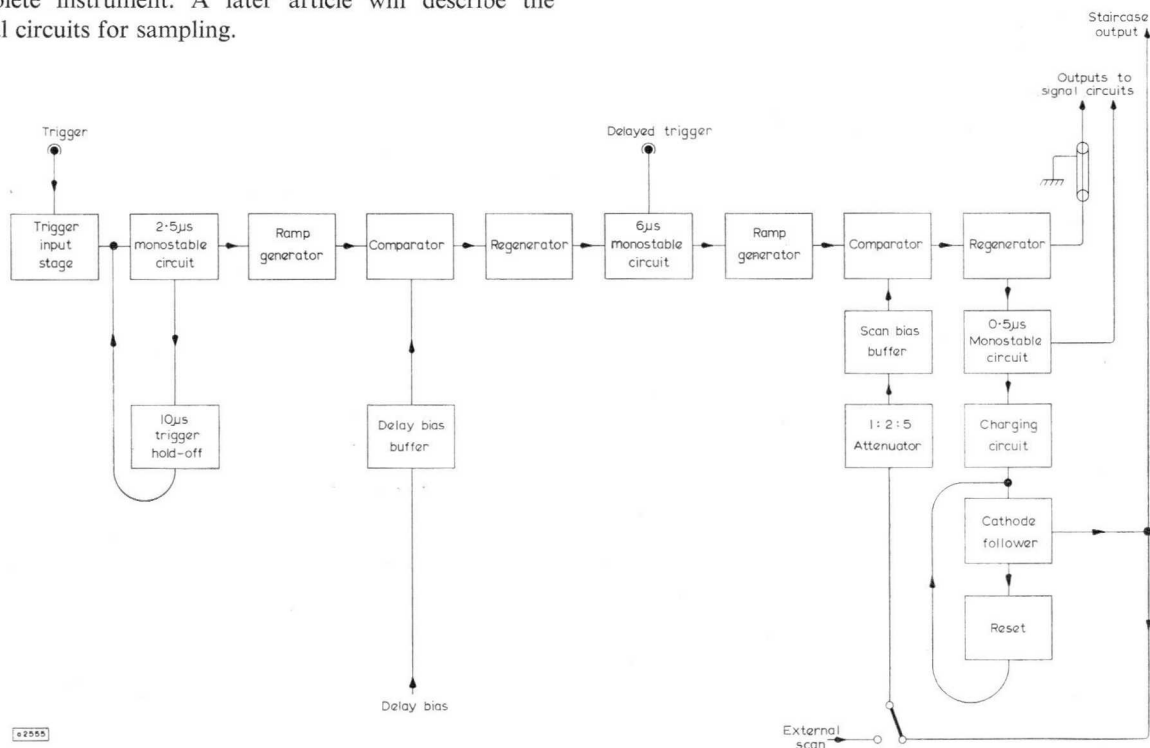


Fig. 1—Block diagram of timing circuits

A full description of sampling systems has been given in a previous article (Ref. 1) but a block diagram of the timing section is given in Fig. 1. The circuits are fired by a trigger pulse which is time-locked to the signal and precedes the part of the signal waveform to be examined. They produce a series of pulses, sometimes called a 'slewed' pulse, whose delay relative to the input trigger progressively increases for each successive trigger. This

a maximum value of about 1µs and a minimum value of about 100ns. In simplified form, the major timing waveforms are shown in Fig. 2. The system described meets the following specifications:

Trigger Requirements

Amplitude: 50mV to 20V for all triggers > 10ns duration or > 0.50Vns area for triggers < 10ns duration.

- Rate: 10c/s to 20Mc/s (hold-off circuit operates above 100kc/s). Randomly spaced trigger pulses can be accepted.
- Polarity: Positive or negative.
- Input capacitance: Approx. 20pF.
- Input resistance: Approx. 5kΩ.
- Trigger Delay**
- Ranges: 100ns or 1μs variation, continuously variable by means of 10-turn Helipot.
- Calibration error: < ±2% of range.
- Minimum delay: < 120ns from normal trigger input socket; < 50ns from 'Delayed Trigger' socket.
- Intrinsic jitter: < 1:10 000, or < 50ps, whichever is greater.
- Delayed trigger output: 3V positive pulse.

Timebase

- Sweep speeds: Ten calibrated sweep speeds from 0.5μs/cm to 0.5ns/cm in 1:2:5 sequence.
- Linearity error: < ±2%.
- Samples per sweep: Approx. 150 to 1500.

The various parts of this circuit shown in block diagram form in Fig. 1 are described more fully below.

CIRCUITS

An important consideration in the design of the circuits of a sampling oscilloscope intended for general use is that they should be aperiodic, that is, the behaviour of the

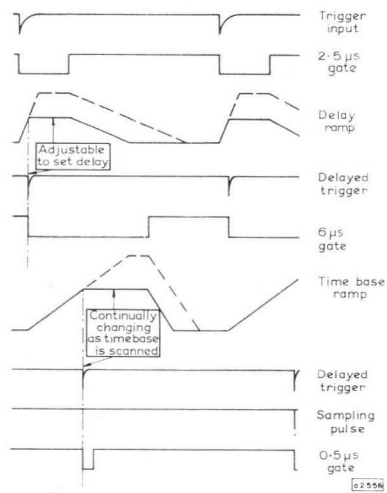


Fig. 2—Major timing waveforms

system following a trigger pulse should be entirely independent of the period between successive triggers, within the design limits. For this reason, the circuits are d.c. coupled, or, in some cases, coupled via time-constants which are small compared to the minimum time between the triggers in that part of the circuit. The design has been greatly facilitated in this respect by the provision of several supply rails.

The circuits are flexible enough to permit the system performance to be changed easily should the need arise.

This results in some sections of the present design being more complicated than is necessary. Some simplifications are, however, suggested later in the article. The circuits shown in Figs. 3 to 13 are fully tolerated and have been reproduced several times. Many of the circuits described have applications other than the original one, and some of these are suggested.

Trigger Input Stage

Fig. 3 shows the circuit of the trigger input stage which comprises the long-tailed pair Tr₁-Tr₂. The input is d.c. coupled to Tr₁ via R₁ and R₃; this network is capacitance-compensated by C₁. The circuit behaves as a slicer to signals greater than 1V(pk) in amplitude, the slicing level being set by RV₁. The collector voltage swing is limited to about 1V by the tail current of 5mA flowing in 220Ω.

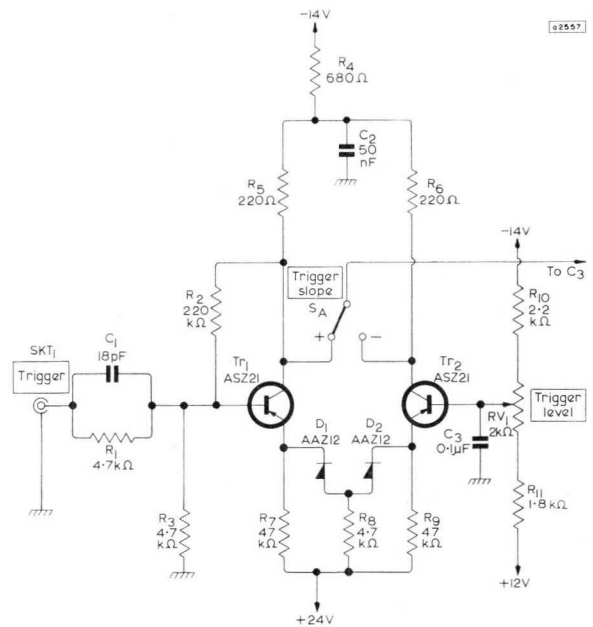


Fig. 3—Trigger input stage

For inputs less than 1V, the stage acts as a unity-gain amplifier. The rise-time of this amplifier is about 4ns which ensures good response to short triggers. The required trigger edge is selected by means of S_A.

The diodes D₁ and D₂ prevent the reverse base-emitter voltage of the transistors being exceeded. This also applies to other circuits where similar diodes appear.

2.5μs Monostable Circuit

The lower half of Fig. 4 shows the 2.5μs monostable circuit which comprises Tr₅, Tr₆ and the constant-current transistor Tr₅₄. Fig. 4 is an emitter-timed monostable circuit, described in detail in Ref. 2, having the 'linear-recovery' system described under the heading 'Modifications' in this reference.

In the quiescent state, Tr₆ and Tr₅₄ are conducting. The collector of Tr₆ is caught at about -1.9V by means of D₈ and Z₂+Z₃. A trigger pulse from the input stage, applied via C₃ and D₃, causes the monostable to switch

into its quasi-stable state, when the collector current (approx. 10mA) of Tr₅₄ is routed into Tr₅ via C₇ and D₄. The diode D₅ remains cut-off.

There is thus produced a positive step of approximately 4V at the collector of Tr₅ and hence at the base of Tr₆. This is shown in waveform W1. (Appendix 3 on page 224 gives notes on the waveforms.) C₇ then charges

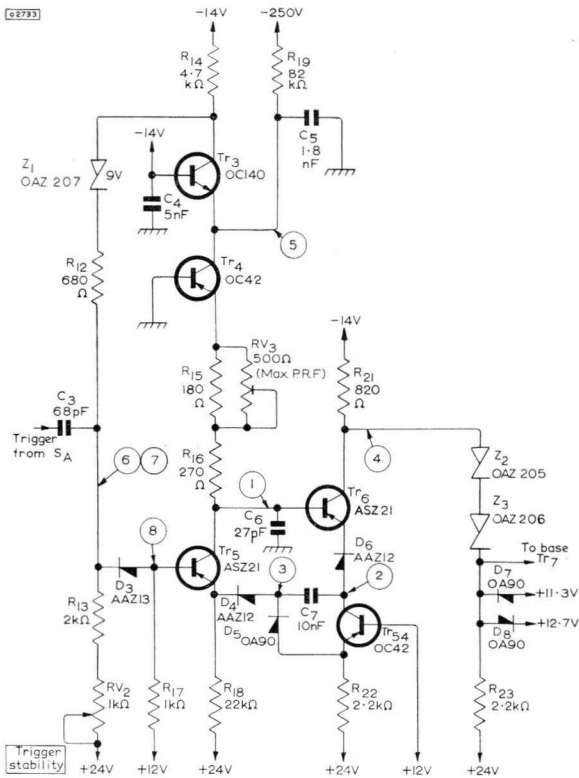


Fig. 4—The 2.5µs monostable circuit and 10µs trigger hold-off

until (after 2.5µs) the emitter of Tr₆ is positive enough to cause the monostable circuit to switch over (waveform W2). During the recovery period which follows, the 4V negative step at the collector of Tr₅ which appears as Tr₅ switches off is coupled via Tr₆, D₆ and C₇ to the cathode of D₅, thus turning it on and reverse-biasing the emitter of Tr₅₄ (waveform W3). The current through R₂₂ thus recharges C₇ almost linearly in a further 2.5µs approx. During the time that Tr₆ is switched off, current through R₂₁ and Z₂+Z₃ turns on D₇, so that the base of Tr₇ (in Fig. 5) switches from +13.2V to +10.8V during the 2.5µs monostable period (waveform W4).

Appendix 1 outlines design considerations on the zener-diode coupling network.

10µs Trigger Hold-off Circuit

A maximum sampling rate of 100kc/s was fixed because of certain considerations in the signal circuits. If the trigger rate exceeds this, the timing circuits must 'count-down'. To ensure reliable triggering under these conditions, a trigger hold-off system comprising Tr₃ and Tr₄ is used, as shown in the upper half of Fig. 4.

With the monostable circuit Tr₅, Tr₆, Tr₅₄ in its quiescent state, the collector current of Tr₅ is about

0.5mA which is a keepalive current through R₁₈. This current also flows out of the collector of Tr₄; the current in R₁₉, however, is greater than 0.5mA, so that the emitter of Tr₃ is forward biased, and caught at -14V. When the monostable circuit fires, the collector current of Tr₄ rises to about 10mA, which exceeds the current available in R₁₉, so that C₅ charges (waveform W5) and Tr₃ is switched off. The positive step which thus appears at the collector of Tr₃ is coupled to the cathode of D₃, blocking the transmission of further triggers to the monostable (waveforms W6, 7 and 8; waveforms W7 and W8 show the blocking action at 1Mc/s).

When the monostable conduction period ends, C₅ discharges via R₁₉ until Tr₃ once again conducts, and allows a further trigger pulse to pass to the monostable

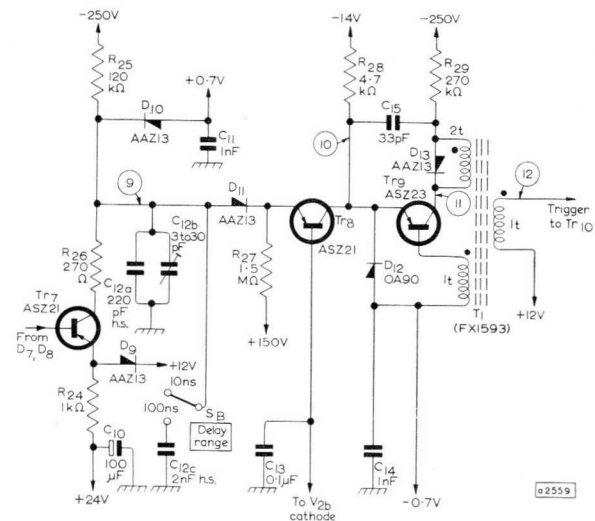


Fig. 5—Delay ramp generator, comparator and regenerator

circuit. Since Tr₄ is not allowed to bottom, the duration of the hold-off period is determined solely by the duration of the monostable period and the ratio of the charge to discharge currents in C₅. In the present circuit, these are 2.5µs and 3:1 respectively, giving a 10µs hold-off.

RV₂ controls the stability and trigger sensitivity of these circuits. When RV₂ is reduced to its minimum value, D₃ is reverse biased by about 2V; no trigger pulses from Tr₁ and Tr₂ are able to overcome this bias, and maximum stability results. At a mid-setting of RV₂, D₃ is just zero-biased, resulting in maximum sensitivity to a trigger pulse. Further rotation causes the system to free-run, at a nominal frequency of 100kc/s adjustable by RV₃, which determines the monostable period.

Delay Ramp Generator and Comparator

The circuit of the delay ramp generator and comparator is shown in the first part of Fig. 5. In the quiescent state, Tr₇ is cut-off. The current through R₂₄ flows into D₉, and the current through R₂₅ from D₁₀. The anode of D₁₁

is thus at approximately +0.2V. A bias applied to the base of Tr_8 , the comparator, holds the emitter at a potential which can be varied between approximately +0.2V and +5.2V. D_{11} is thus reverse-biased.

The negative pulse from the monostable circuit on the base of Tr_7 switches Tr_7 on, and the collector current rapidly rises to approximately 12mA, defined by R_{24} . Since this exceeds the current in R_{25} , C_{12} begins to charge and D_{10} becomes reverse-biased. Above a potential of 10.5V the charging of C_{12} is very nearly linear. Tr_8 turns on after a time determined by the value of the charging current, the value of C_{12} and the bias voltage on the base of Tr_8 .

At the end of the monostable conduction period, C_{12} discharges via R_{25} until D_{10} 'catches'. Two ranges are provided, giving a delay variation of 100ns or 1 μ s for a bias variation of approximately 5V. The delay is set by means of the delay multiplier Helipot RV_9 (Fig. 6). Start and stop limits are adjusted by means of RV_7 and RV_8 .

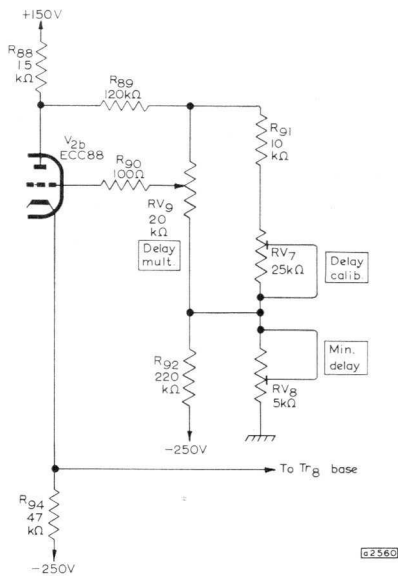


Fig. 6—Delay multiplier and buffer amplifier

The cathode-follower V_{2b} is used to minimise loading on RV_9 and thus ensure good linearity of the multiplier scale. The linearity of the ramp generated by the circuit of Fig. 5 is discussed in Appendix 2 on page 222. Waveform W9 shows the voltage across C_{12} on the 1 μ s delay range and waveform W9a corresponds to the 100ns range.

Regenerator Circuit

The avalanche transistor, Tr_9 in Fig. 5, is used to produce a standard trigger pulse to fire the following stage, from the positive step which appears at the collector of Tr_8 . In the quiescent state, the current in R_{28} holds D_{12} in conduction; the emitter of Tr_9 is thus reverse-biased. Its collector remains at the avalanche potential of about -25V. When Tr_8 switches on, the emitter of Tr_9 is forward-biased (waveform W10) causing avalanche regeneration around the loop formed by Tr_9 , Tr_1 and C_{15} . This produces a narrow negative spike at the output

winding (waveform W12). A feedback winding in the base improves the stability of the output pulse against variations in the speed of the edge from Tr_8 as the TIME/CM control is varied.

Tr_9 remains bottomed until the end of the monostable period, when C_{15} recharges via R_{29} until the avalanche potential is reached (waveform W11), and D_{13} prevents positive overshwing on the output pulse.

6 μ s Monostable Circuit

The monostable circuit Tr_{10} and Tr_{11} (Fig. 7) produces a 6 μ s negative pulse on the base of Tr_{12} after receiving a trigger pulse from T_1 . It is essentially the same in operation at the 2.5 μ s monostable circuit. However, stability of pulse duration is not as important as in the 2.5 μ s circuit (which must synchronise up to several tens of megacycles), and the constant current transistor is therefore not required. In addition, a fast recovery of less than 4 μ s must follow the quasi-stable period, for the

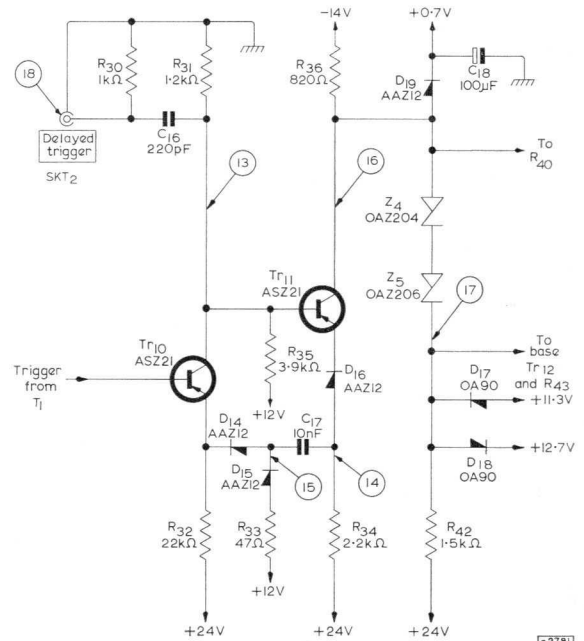


Fig. 7—The 6 μ s monostable circuit

circuit to work up to 100kc/s. For this reason, the recovery-path resistor R_{33} is reduced to the minimum value permitted by the peak collector current rating of Tr_{11} , ensuring a rapid discharge of C_{17} .

The socket SKT_2 enables positive trigger pulses of amplitude > 1V and having a p.r.f. \leq 100kc/s to be applied directly to this monostable circuit, thus by-passing the fixed minimum delay present in the above circuits. In this way, a minimum delay of approximately 50ns can be achieved on timebase ranges \leq 5ns/cm. Alternatively, the 3V positive-going pulse which appears at this socket when the monostable fires can be used to trigger an external circuit (waveform W18). In this mode, for example, the STABILITY control can be rotated fully clockwise, and the instrument becomes its own pulse generator at 100kc/s. The waveforms for this circuit are shown in W13 to W18.

Timebase Ramp Generator and Comparator Circuit

The circuits of the timebase ramp generator and comparator, shown in Fig. 8, are essentially the same as those of Tr₇ and Tr₈ described above. One major difference is the addition of Tr₁₃. This is required to discharge the largest timing capacitor (C_{19d}, providing the 0.5, 0.2 and 0.1 μs/cm ranges), since the discharge current through R₃₇ is insufficient to restore the ramp generator to its quiescent state within the 10 μs minimum cycle-time. Tr₁₃ is turned on by the overswing of voltage which appears at the collector of Tr₁₁ as the monostable recovers. Its collector current is defined by R₄₆ and is sufficient to discharge C_{19d} in about 2 μs (waveforms W22 and W23).

Only three basic ramp durations are generated; these are 5 μs, 0.5 μs and 50 ns (waveforms W19a to W19d). Range interpolation in a 1:2:5 sequence is achieved by scanning all, 2/5, 1/5 or 1/10 of the total ramp. The

that the available recharge time may be only 4 μs, necessitates an increased value of discharge current, and this is ensured by reducing the collector resistor R₄₉ to 150 kΩ.

The waveforms from this circuit are shown in W20, W21 and W24, the latter showing a single output pulse. The amplitude of the output pulse is constant within ±1% over the whole of the timebase range.

0.5 μs Monostable and Buffer Stages

A 0.5 μs pulse is required at each sample-time for the following purposes:

- (i) To step up the staircase generator
- (ii) To operate the 'reference charge' generators (Refs. 1 and 3)
- (iii) To gate on the amplifiers in the signal circuits (Refs. 1 and 3)

The circuit is shown in Fig. 10.

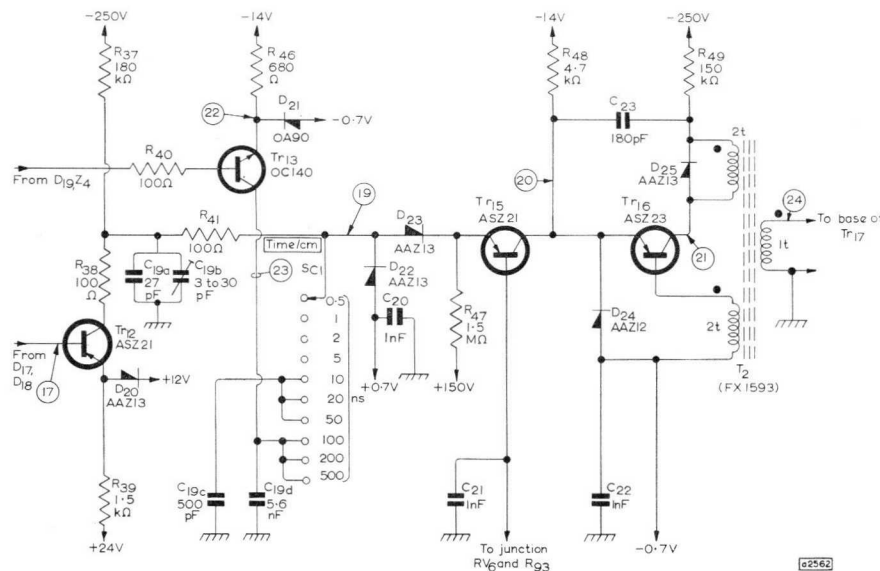


Fig. 8—Timebase ramp generator, comparator and regenerator. The output of T₂ also connects to the signal circuit

system comprising S_{e2}, R₈₀, R₈₁, R₈₂ and R₈₃ (Fig. 9) sets the fraction to be scanned by attenuating the staircase voltage (7.15 peak-to-peak) from the staircase generator. RV₆ sets the minimum value of the scanning voltage, and hence determines the 'get-away delay' of the timebase.

S_E has been included to permit the use of either a 10cm or 7cm calibrated graticule on the display c.r.t. In the 7cm position, the resistor R₈₄ scales down every timebase range by a factor 0.7, so that each centimetre division may be made to correspond to the time marked on the TIME/CM control even though a display of reduced size is used. By suitable choice of R₈₄, any graticule length less than 10cm can be catered for.

Regenerator Circuit

The output regenerator, Tr₁₆, also shown in Fig. 8, is similar to the regenerator described above, and serves the same purpose, namely, to provide a standard output trigger pulse to drive the following circuits. A larger feedback capacitor (C₂₃) is used, to provide a pulse of sufficient amplitude into a 100 Ω line. This, and the fact

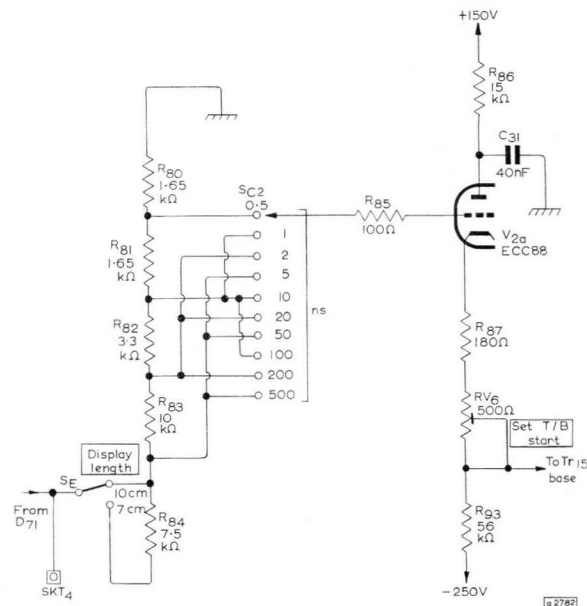


Fig. 9—Range interpolator and buffer amplifier

Tr₁₇ and Tr₁₈ form an emitter-timed monostable circuit producing a 0.5μs pulse on receipt of a trigger from T₂. In the quiescent state D₂₉ and D₃₀ are forward biased, because of the currents through R₅₅ and R₅₈. Points G₁ and G₂ are, therefore, caught at -0.5V while Tr₁₉ and Tr₂₀ are cut off, and their collectors are at -14V. During the monostable period, the collector current of Tr₁₇ (approximately 10mA) divides in R₅₆ and R₅₇, turning

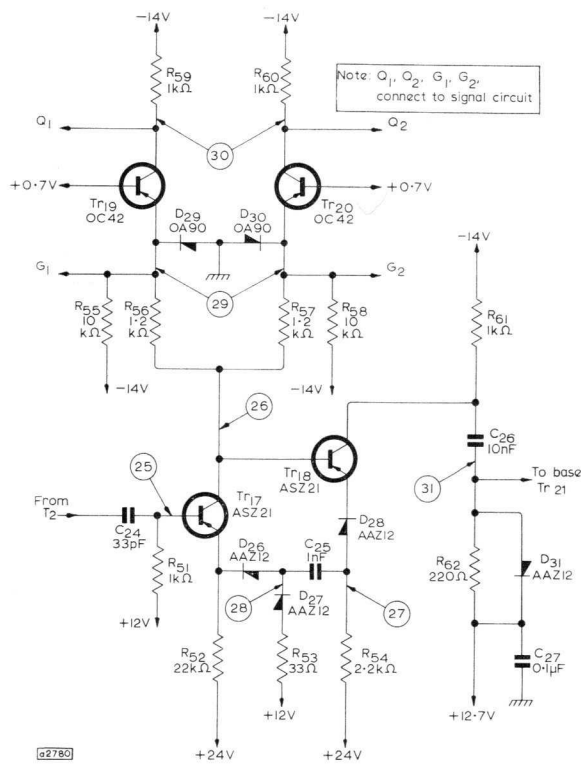


Fig. 10—The 0.5μs monostable circuit and buffer amplifier

on Tr₁₉ and Tr₂₀ and reverse-biasing D₂₉ and D₃₀. The points G₁ and G₂ thus carry positive pulses of 0.5μs duration between the limits -0.5V and +1V (waveform W29). The points Q₁ and Q₂ also carry positive pulses starting at -14V and rising to a value determined by the setting of the reference charge controls (waveform W30). Typical waveforms for this monostable are shown in W25 to W28.

Staircase Generator Circuit

The staircase generator circuit is in three parts; the charging circuit, the resetting circuit, and the blanking amplifier. Fig. 11 shows the charging circuit.

The collector of Tr₁₈ is coupled via C₂₆ to the base of Tr₂₁ which thus switches on for 0.5μs during each sampling cycle (waveform W31). The emitter current is determined by S_D, and has a maximum value of 4.5mA and a minimum value of 0.25mA giving a range of sampling densities from approximately 15 to 150 dots per cm. The collector of Tr₂₁ is normally held at a potential slightly negative to that across C₂₈, via R₆₆ and the cathode follower V₁. The diode D₃₄ is, thus, reverse-biased. When Tr₂₁ is

switched on, D₃₄ conducts, and a short pulse (waveform W32) is injected into C₂₈ which charges up through one step.

The charge on C₂₈ decays slowly during the inter-trigger periods, because of leakage currents; these are minimised by using silicon diodes. A cathode-follower is essential here as an output buffer. The maximum period between steps can be extended to over 1s before the

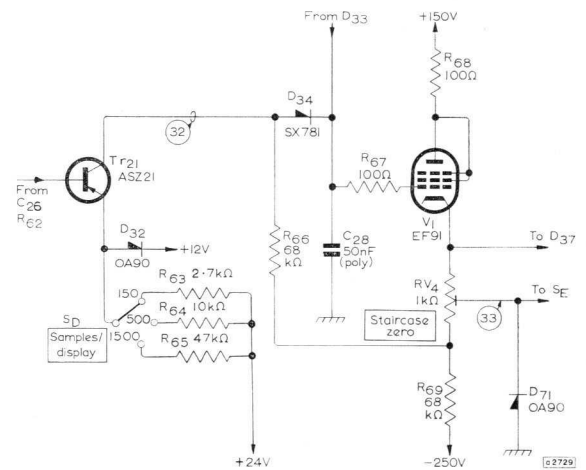


Fig. 11—Staircase charging circuit

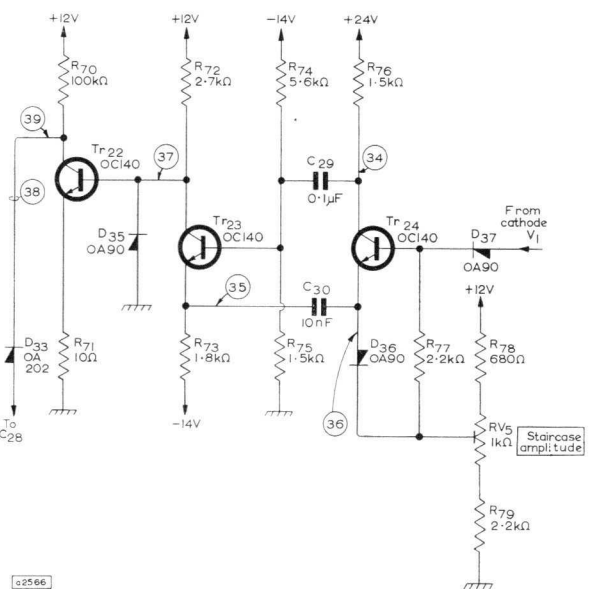


Fig. 12—Staircase reset monostable circuit

droop on each step becomes excessive. The minimum period is determined to some extent by the hole-storage in D₃₄, and therefore a low minority carrier storage diode type SX781 is used. The linearity of the generated waveform is very good, as shown in waveform W33, and the linearity error can be calculated using the expressions derived in Appendix 2.

D₇₁ is included to prevent a lock-out around the system Tr₁₅, Tr₁₆, Tr₁₇, Tr₂₁ and V₁; such a lock-out can cause a long delay, subsequent to the equipment

being switched on, before the staircase generator can operate. The probable sequence of events which lead to a lock-out in the absence of D_{71} is as follows. During the warm-up period, the grid current of V_1 charges C_{28} to a negative potential. When this period is over, the cathode of V_1 remains fairly negative, so that the comparator is always cut off. No trigger pulses reach the pump monostable circuit, so that the charge on C_{28} must be allowed to leak away before the loop can become active. If the leakage currents are unfavourable, a stable lock-out state can result.

The resetting circuit is shown in Fig. 12. After the selected number of steps have been generated, D_{37} conducts and triggers the emitter-timed monostable Tr_{23} and Tr_{24} . The precise trigger level (and hence the staircase amplitude) is set by RV_5 . The $5\mu s$ positive pulse at the collector of Tr_{23} turns off Tr_{22} , which discharges C_{28} via D_{33} . The whole resetting operation always takes place before Tr_{21} produces the next pulse. The waveforms of the resetting monostable circuit are shown in W34 to W39.

Blanking Amplifier

The blanking amplifier circuit is shown in Fig. 13. Tr_{14} is a bottoming amplifier driven by the negative waveform from the $6\mu s$ monostable circuit (Fig. 7). The Tr_{14} collector voltage swing of approximately 25V is coupled via the transformer T_6 to sockets, to which connections

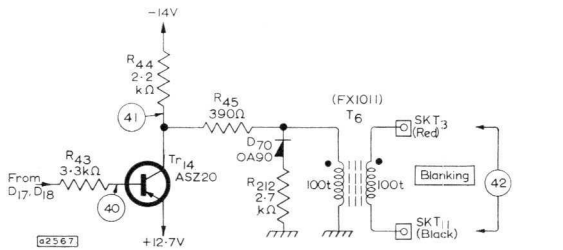


Fig. 13—Blanking amplifier

to the grid or cathode of the display c.r.t. can be made, to provide blanking of the display. This suppresses some short transients which unavoidably appear on the y-deflection voltage during each sampling period, and tend to cause an apparent thickening of the trace, especially at the highest y-sensitivity settings, and at high p.r.f.

The waveforms of this circuit are shown in W40 to W42. Note that the heavy bottoming of Tr_{14} causes stretching of the voltage pulse to about $8\mu s$.

POSSIBLE MODIFICATIONS

Since the above circuits were designed (mid-1961), several improvements or alternative arrangements have become apparent. These modifications result in improved performance and greater simplicity or both. Some of the supply rails are also unnecessary.

Delay Circuit

A separate ramp generator for the delaying function was originally used, since this permits the trigger delay to be independent of the timebase range. However, it is questionable whether this is advantageous. An alternative method is to use a single ramp for both trigger delay and

timebase purposes, as shown in Fig. 14. This permits a delay variation of (say) ten times the basic 'TIME/CM' value. A single ramp system is now the preferred arrangement in most commercial instruments. One manufacturer has modified the timing unit in this way to offer better delaying facilities (for example see Ref. 4.)

The advantages of such a method are that since none of the components used in the delay circuits (above) are required, a more economical system is achieved while at the same time a lower value of minimum delay is obtained.

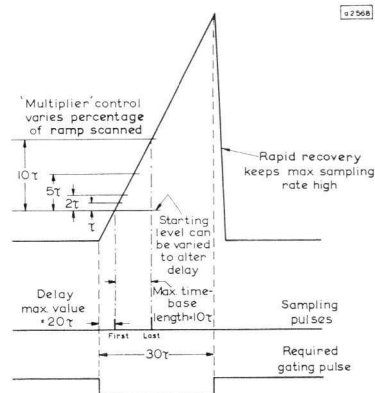


Fig. 14—Single ramp system

The second of these advantages is particularly important where the trigger is derived from the signal waveform, since then the signal must be passed through a delay cable, which unavoidably distorts the pulse shape. The longer the starting delay in the timebase, the greater is this distortion. With the method suggested, a minimum delay

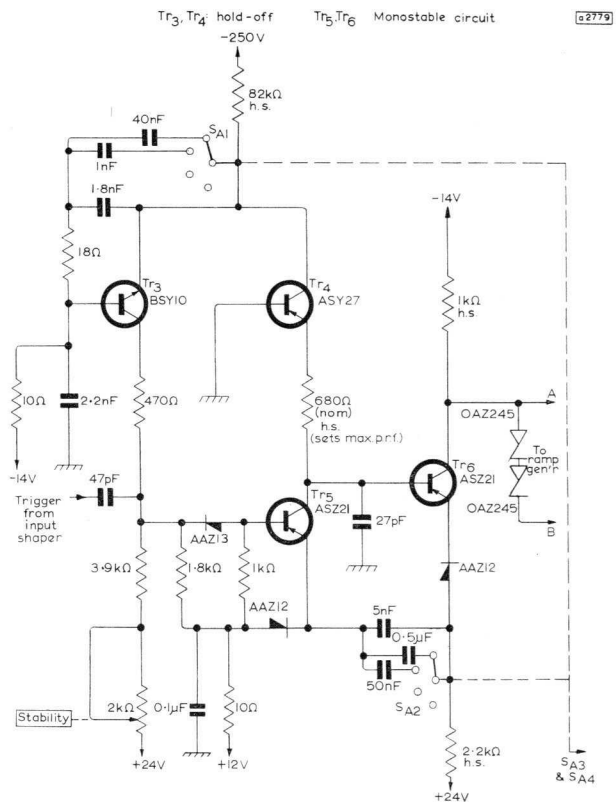


Fig. 15a—Improved timebase: monostable circuit and hold-off circuit

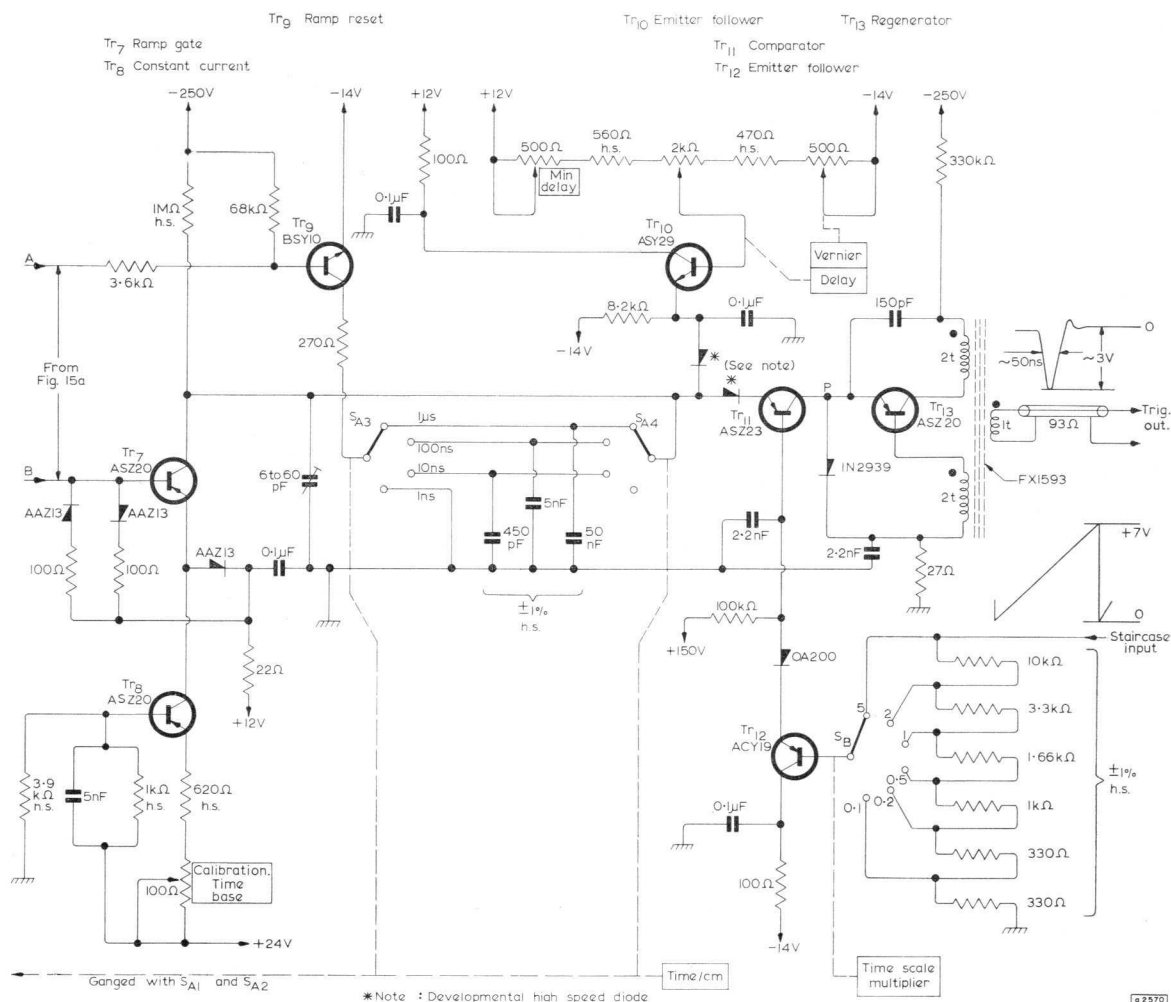


Fig. 15b—Improved timebase: generator and comparator

of $< 45\text{ns}$ has been achieved. In addition, it has been found that a much smaller part of the timebase ramp than that used in the present circuit (10% on the 0.5ns/cm range) can be scanned. For example, a stable timebase of 1ns (that is, 0.1ns/cm) can be obtained quite reliably by scanning a 0.1% portion of a $1\mu\text{s}$ ramp. In this way, the number of basic ramps could be greatly reduced, resulting again in a simpler and more economical design.

A slightly modified circuit is required in the first monostable circuit and trigger hold-off, since this must produce pulses long enough to gate the particular ramp being generated. The hold-off period, however, need not always be four times the gating period, since this will reduce the maximum trigger frequency unnecessarily.

The results obtained with this system have been very satisfactory. The circuit of the improved timebase section are shown in Figs. 15a and 15b; it should be noted that these circuits are not fully tolerated and are shown only to indicate the simplification which results from the use of a single ramp (eleven transistors replace the original fourteen transistors and two triodes).

The system performance is as follows:

BASIC TIMES/CM: $1\mu\text{s}, 100\text{ns}, 10\text{ns}, 1\text{ns}$
SCALE MULTIPLIER: $\times 5, \times 2, \times 1, \times 0.5, \times 0.2, \times 0.1$

OVERALL RANGE: $5\mu\text{s/cm}$ to 100ps/cm
DELAY VARIATION: 150 times basic TIME/CM value

MIN. DELAY: $< 45\text{ns}$ below 50ns/cm
JITTER: $< 1:1000$, or $< 30\text{ps}$, whichever is greater

MAX. REP. RATE: 100kc/s on 10ns and 1ns ranges
 25kc/s on 100ns range
 2.5kc/s on $1\mu\text{s}$ range

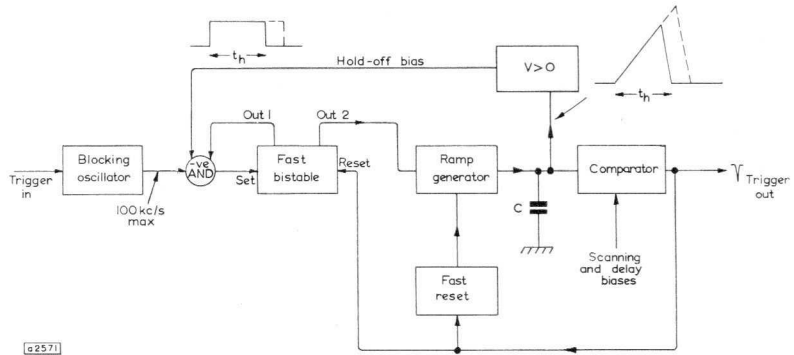
(The scale multiplier does not affect max. rep. rate)
MAX. SYNC. FREQUENCY: $> 50\text{Mc/s}$ in input circuit in Fig. 3, on ranges below 10ns/cm (see below).

S_A and S_B could be replaced by one switch giving 15 calibrated ranges between $5\mu\text{s}$ and 100ps/cm , although

there is some advantage in the extra flexibility permitted by the separate 'MULTIPLIER' control.

The avalanche generator, Tr_{13} , introduces a delay of up to 20ns, which is a large proportion of the overall delay. This might be reduced by replacing the regenerator by a $0.5\mu s$ blocking oscillator connected directly to point 'P', which would also generate the gating waveforms at present generated by Tr_{17} to Tr_{20} of Fig. 10. The diode in the collector of Tr_{11} produces a 400mV step of sub-

Fig. 16—Alternative system



stantially constant speed and improves the stability of output pulse amplitude against range-changes, and also reduces jitter on the slower ranges.

In this circuit, several other improvements are made. The use of a constant current transistor, Tr_8 , to supply the ramp gating transistor, Tr_7 , results in the sweep calibration being linearly dependent on the voltage of the +24V line, and this line only. By arranging for the staircase amplitude to be also linearly dependent on the +24V line voltage, the timebase length is substantially independent of all supply line voltages.

The valve V_2 is replaced by the emitter-followers Tr_{10} (delay) and Tr_{12} (scan) with consequent saving in power requirements.

It has been found that imperfect decoupling of supply lines leads to 'base-line wiggles' on the final display when viewing at maximum sensitivity. The decoupling networks have therefore been improved.

In another possible arrangement the monostable circuit is replaced by a bistable circuit as shown in Fig. 16. Here, the hold-off period lasts just long enough for the ramp to reach the current value of the scanning bias and reset to zero, when the next trigger is applied. Higher repetition rates on longer timebase ranges could probably be achieved in this way. The trigger input blocking oscillator limits the upper frequency to 100kc/s.

C.R.T. Blanking

The transients on the transformed signal output (Ref. 3) last for 1 to $2\mu s$ after each sample. The c.r.t. trace should be blanked-out during this interval. With the present circuit, blanking starts at the beginning of the timebase and lasts for about $8\mu s$. Thus, an unnecessarily long blanking interval is used, and some brightness variation over the scan on slow sweeps might result. A better method would be to make Tr_{14} and T_6 (Fig. 13) into a $2\mu s$ blocking oscillator which is fired at the beginning of each sample.

Staircase Reset

A $5\mu s$ blocking oscillator could replace the present $5\mu s$ emitter-timed monostable circuit, which resets the staircase to zero, resulting in greater simplicity and perhaps lower cost.

Scanning System

In the present circuit, the scanning voltage is derived from the staircase generator. However, there is no reason

why an externally generated waveform of the right amplitude and d.c. level should not be used for scanning. Alternatively, scanning can be achieved by manual rotation of a suitable control. Also, the sampling densities can be varied continuously by replacing S_D (Fig. 11) by a variable resistor. Finally, a continuous variation of the effective sweep-speed can be provided by varying the division ratio to the comparator.

A modification which introduces all of these facilities is shown in Fig. 17. The variable resistor RV_1 serves a different purpose in each of the three positions of S_D , which is now used to select the scanning mode. RV_2 increases the effective sweep-speed by a factor of up to 3 times.

Trigger Input Circuits

Various improvements to the trigger input circuits are suggested. The trigger delay could be reduced and high-frequency synchronising performance improved by the use of a tunnel diode trigger circuit. With a 1N2939, for example, synchronisation up to 250Mc/s has been achieved. A simple emitter-follower preceding the trigger input stage could be added to the circuit of Fig. 3 to achieve a higher trigger sensitivity, whilst the input impedance would be raised to about $100k\Omega$ in parallel with $5pF$ to $10pF$.

OTHER APPLICATIONS OF THE CIRCUITS

Staircase Generator

The staircase generator can be used to produce from two to more than 50 000 steps per cycle anywhere in the input frequency range 1c/s to 1Mc/s, by suitable choice of the charging current, charging-pulse duration, storage capacitor, etc. The amplitude can range from 1V to over 30V simply by varying the reset trigger voltage. (For the higher amplitudes, Tr_{21} should be changed to ASZ20, and the reset monostable circuit modified slightly.) This wide range of operation, coupled with excellent linearity,

makes the circuit suitable for many systems requiring an accurate staircase waveform.

By replacing the pump circuit Tr_{21} , D_{34} and R_{66} by a p-n-p silicon transistor arranged as a constant current generator, this circuit may be modified into a wide-range current (or voltage) controlled oscillator, producing a very linear sawtooth with a 2 to $3\mu s$ 'flyback' time over the range 0.05c/s to 50kc/s. Measurements indicate a linear current-frequency law over at least five decades, and a

any supply-rail variations cause proportional changes in the rate-of-rise of the ramp and the comparator bias as in Fig. 15b. However, in the original circuits described this dependence is not excessive, and with straightforward supply-line regulators the stated accuracy of $\pm 2\%$ can be maintained for mains voltage changes of $\pm 10\%$.

Monostable Circuit

It is pointed out in Reference 2 that the emitter-timed

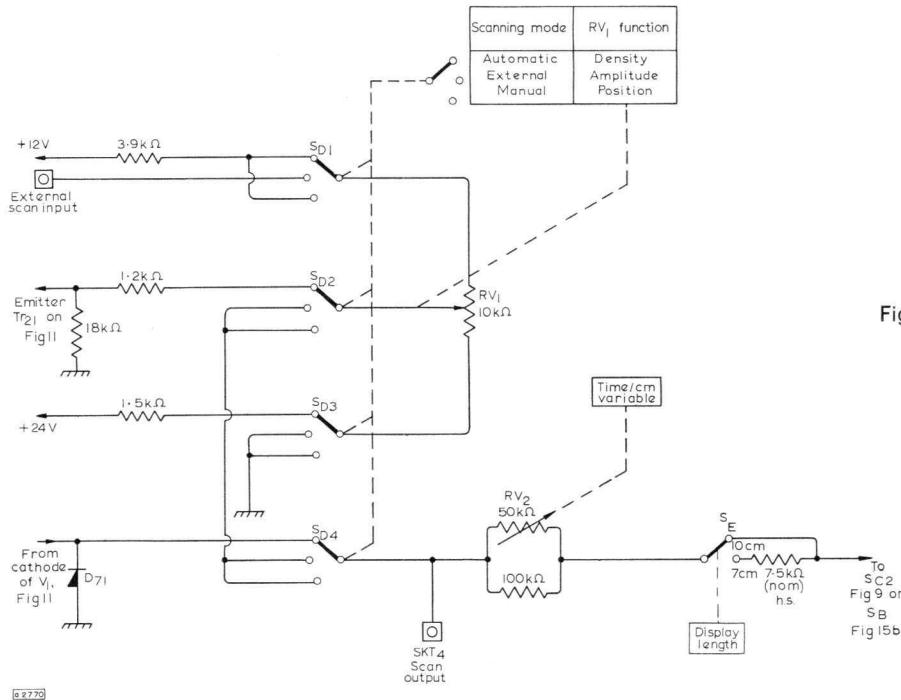


Fig. 17—Modified scanning mode control

linear voltage-frequency law over about two decades, using a simple emitter-stabilised configuration for the constant-current generator.

Delay Circuit

The present delay circuit has two delay ranges giving variations of 100ns and $1\mu s$. However, these ranges can easily be extended, and full-scale delay variations from 10ns to several milliseconds can be obtained. The long recovery time of the delay ramp generator (Fig. 5) can be a disadvantage, especially on very long delay ranges, in which case the rapid recharging method of the timebase circuit (Fig. 8) might be used.

The linearity of delay as a function of comparator bias is good. (See Appendix 2, page 222.) Jitter is low, and a delay value of $< 10^{-4}$ times the range period is typical. This might be improved by increasing the ramp amplitude, so as to reduce the effects of pick-off noise.

The output trigger pulse is independent of the delay range, and is a narrow negative pulse at low impedance, the amplitude and duration of which can be adjusted by means of the feedback capacitor (C_{15} in Fig. 5).

A disadvantage of the circuit is that the calibration accuracy depends on the stability of the supply-rail voltages. An alternative arrangement is one in which

monostable circuit can be used as a linear sawtooth generator. This feature, together with the high trigger sensitivity, makes the circuit very useful as a timebase circuit for a conventional oscilloscope. With a high-voltage high-speed transistor such as the ASZ20 or BSY10 (n-p-n), sawtooth waveforms of good linearity and several tens of volts amplitude can be obtained down to the microseconds region.

The addition of a trigger input stage and a trigger hold-off circuit as shown in Figs. 3 and 4 (with modified component values) provides the basis for a versatile timebase generator (Ref. 5). Long sweep times, however, are difficult to obtain in this way.

REFERENCES

1. GILBERT, B., 'Sampling Techniques Applied to High-Speed Pulse Oscillography'. **Mullard Technical Communications**, Vol. 5, No. 48, June 1961, pp. 317 to 329.
2. GILBERT, B., 'Emitter-Timed Monostable Circuit'. **Mullard Technical Communications**, Vol. 5, No. 49, July 1961, pp. 345 to 354.
3. GILBERT, B., 'A Feedback Sampling Oscilloscope Channel'. An article to be published in **Mullard Technical Communications**.
4. CARLSON, R., 'A Versatile New DC-500Mc Oscilloscope with High Sensitivity and Dual Channel Display', **Hewlett-Packard Journal**, Vol. 11, No. 5-7, pp. 1 to 8, Jan.-Mar. 1960.
5. GILBERT, B., 'Timebase Circuits Using the BSY10 Transistor'. An article to be published in **Mullard Technical Communications**.

APPENDIX 1

Current-mode Coupling Network

It is often necessary to couple two switching transistors in such a way that the most efficient use is made of the collector current of the first transistor in switching on or off the second transistor. The time taken for the second transistor to switch is dependent on the amount of transient current available to charge or discharge its base and the associated capacitances. Where d.c.-coupling is also required for a particular reason, and a voltage shift must be introduced, a zener-diode coupling network is frequently used. Examples of this occur in Figs. 4 and 7, and the generalised circuit is shown in Fig. 18.

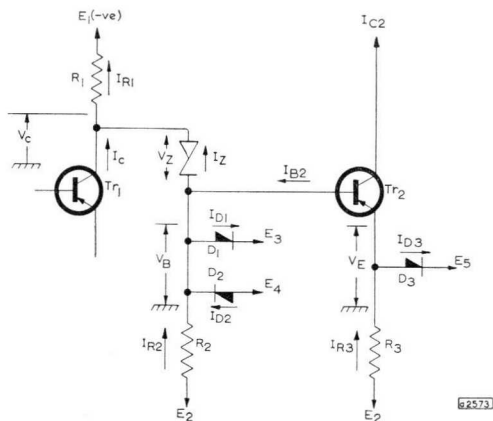


Fig. 18—Zener diode coupling networks

Tr₁ and Tr₂ are assumed to be emitter-current-switched stages, in which the collector current is independent of the collector circuit conditions, provided that the transistor does not bottom.

Definitions

The ON and OFF states are defined as follows:

- ON state: Tr₂ is conducting, and its emitter current is defined by R₃. D₂ is forward biased and Tr₁ is at its lowest value of collector current (or cut off).
- OFF state: Tr₂ is cut off, D₁ is forward biased, Tr₁ is at its highest value of collector current.

In addition to the symbols shown in Fig. 18, the following are defined:

- V₁ = forward bias voltage across D₁ during OFF state
- V₂ = forward bias voltage across D₂ during ON state
- V₃ = forward bias voltage across D₃ during OFF state
- V_{EB} = forward bias emitter voltage of Tr₂ during ON state
- V_Z = reverse breakdown voltage of the zener diode.

These terms are current-dependent, but will be considered as constant for simplicity. In a practical calculation, the values at the anticipated current levels are used:

- I_{D1} = forward current in D₁ during OFF state
- I_{D2} = forward current in D₂ during ON state
- I_E = required value of emitter current of Tr₂ during ON state.

The subscripts ON and OFF will be used to denote the value of a variable in a given state. Leakage currents are neglected, since they are normally small compared with the practical values of currents associated with the network.

Conditions

The following conditions must be satisfied for the network to operate correctly.

- (i) I_Z > 0, to ensure that the zener diode is in reverse conduction at all times.
- (ii) I_{D1} > 0 and I_{D2} > 0 to define catching potentials.
- (iii) V_{C(ON)} and V_{C(OFF)} must each fall between specified limits, to ensure that the requirements for the rest of the circuit associated with Tr₁ are met.
- (iv) V_{B(OFF)} must be more positive than E₅+V₃, to ensure that Tr₂ is cut off during OFF state.
- (v) V_{B(ON)} must be more negative than E₅-V_{EB} to ensure that D₃ is reverse-biased during ON state.
- (vi) The ratio of the transient base currents in Tr₂ during switch-on and switch-off period will determine the ratio of switch-on to switch-off time, and must be chosen to suit the requirements. Let this ratio be called K.

Equations

It can be simply shown that the following expressions give the values of the unknown quantities E₃, E₄, V_Z, R₁, R₂ and R₃ in terms of the known quantities.

$$(i) \quad E_3 > E_5 + V_3 - V_1 \quad \dots(1)$$

$$E_4 < E_5 + V_2 - V_{EB} \quad \dots(2)$$

Note These catching rails will usually be kept to the minimum value required for correct operation to reduce delay time and the time taken for the emitter current of Tr₂ to reach its final value. This is because of stray capacitances.

$$(ii) \quad V_Z = E_4 - V_2 - V_{C(ON)} \quad \dots(3)$$

or

$$V_Z = E_3 + V_1 - V_{C(OFF)} \quad \dots(4)$$

Note It is assumed that only V_{C(ON)} or V_{C(OFF)} must be specified, since in practice the voltage swing V_{C(OFF)}-V_{C(ON)} is small. If it is necessary for some reason to define both V_{C(ON)} and V_{C(OFF)}, the minimum value of E₃ required to ensure cut-off of Tr₂ during the OFF state would first be calculated from Eq(1), then V_Z from Eq(4) and finally E₄ from Eq(3).

$$(iii) \quad R_3 = \frac{E_2 - E_4 + V_2 - V_{EB}}{I_E} \quad \dots(5)$$

$$(iv) \quad R_1 = \frac{V_{C(OFF)} - E_1}{I_{Z(OFF)} + I_{C(OFF)}} \quad \dots(6)$$

Notes (a) E₁ is a negative supply rail, and R₁ is thus positive.

(b) I_{Z(OFF)} is the minimum value of zener current at which it is desired to operate, that is, at a value well in the constant-voltage region of the diode.

$$(v) \quad R_2 = \frac{[(V_{B(OFF)} - E_2)(1+K) - \Delta V_B]R_1}{V_B - R_1[1+(1+K)I_{Z(OFF)}]} \quad \dots(7)$$

where ΔV_B = voltage swing on base of T₂
= E₃-E₄+V₁+V₂,

V_{B(OFF)} = voltage on base of Tr₂ during off state
= E₃-V₁,

and I = I_{C(OFF)}-I_{C(ON)}-(1-α₂)I_E ... (8)

Notes (a) I_{C(OFF)} corresponds to the maximum value of the collector current of Tr₁.

(b) α₂ = the large signal alpha of Tr₂.

(c) This expression will only hold for K if ΔV_B is kept to the minimum value required to switch Tr₂.

Example

Suppose the known quantities to be as follows:

- $V_1 = V_2 = V_3 = 0.5V$
- $V_{EB} = 0.25V$
- $V_{C(OFF)} = -3.0V$
- $E_1 = -14V$
- $E_2 = +24V$
- $E_5 = +12V$
- $I_{Z(OFF)} = 1mA$ (minimum desired zener current)
- $I_{C(ON)} = 0.4mA$
- $I_{C(OFF)} = 10mA$
- $\bar{\alpha}_2 = 0.95$ (minimum value)
- $K =$ unity

From (1)

$$E_3 > +12 + 0.5 - 0.5$$

Put $E_3 = +12.5V$, giving 0.5V margin

From (2)

$$E_4 < +12 + 0.5 - 0.25$$

Put $E_4 = 11.75V$, giving 0.5V margin

Therefore

$$V_{B(ON)} = +11.25V$$

and

$$V_{B(OFF)} = +13V$$

and

$$V_B = 13 - 11.25 = 1.75V$$

From (4)

$$V_Z = 12.5 + 0.5 - (-3) = 16V$$

From (5)

$$R_3 = \frac{+24 - 11.75 + 0.5 - 0.25}{12} = 1.04k\Omega \text{ (say } 1k\Omega)$$

From (6)

$$R_1 = \frac{-3 - (-14)}{1 + 10} = 1k\Omega$$

From (8)

$$I = 10 - 0.4 - (1 - 0.95)12 = 9mA$$

From (7)

$$R_2 = \frac{[(13 - 24)(1 + 1) - 1.75]}{1.75 - 1[9 + (1 + 1)1]} \cdot 1 = 2.57k\Omega$$

From these results, the values of the maximum and minimum currents in R_1 and R_2 , the maximum current in the zener diode and the catching currents in D_1 and D_2 can be found:

$$I_{R1(OFF)} = \frac{(-V_Z + V_{B(OFF)} - E_1)}{R_1} = \frac{[-16 + 13 - (-14)]}{1} = 11mA$$

$$I_{R1(ON)} = \frac{(-V_Z + V_{B(ON)} - E_1)}{R_1} = \frac{-16 + 11.25 - (-14)}{1} = 9.25mA$$

$$I_{R2(OFF)} = \frac{(E_2 - V_{B(OFF)})}{R_2} = \frac{24 - 13}{2.57} = 4.28mA$$

$$I_{R2(ON)} = \frac{(E_2 - V_{B(ON)})}{R_2} = \frac{24 - 11.25}{2.57} = 4.97mA$$

$$I_{Z(ON)} = I_{R1(ON)} - I_{C(ON)} = 9.25 - 0.4 = 8.85mA$$

$$I_{D1} = I_{R2(OFF)} - I_{Z(OFF)} = 4.28 - 1 = 3.28mA$$

$$I_{D2} = -I_{R2(ON)} - I_{Z(ON)} + (1 - \bar{\alpha}_2)I_E = -4.97 + 8.85 - 0.6 = 3.28mA$$

The last two calculations provide a check on the value of K .

It can be shown that the effect of increasing R_2 to 2.7k Ω (the nearest preferred value in the 10% range) is to increase K to 1.32, resulting in a slightly better switch-on time.

APPENDIX 2

An Examination of the Sources of Non-linearity in a Ramp Generated by a 'Constant-current Transistor' Circuit

The basic circuit is shown in Fig. 19, and practical examples occur in Figs. 5, 8 and 15b. Resistor R_1 supplies a current which holds D_2 conducting during the quiescent state and recharges C during the recovery period. (Note that in the practical circuits of Figs. 8 and 15b, recharging time is reduced by the use of an extra transistor.) The resistor R_c serves to reduce the Q of a possible tuned circuit formed by C and stray

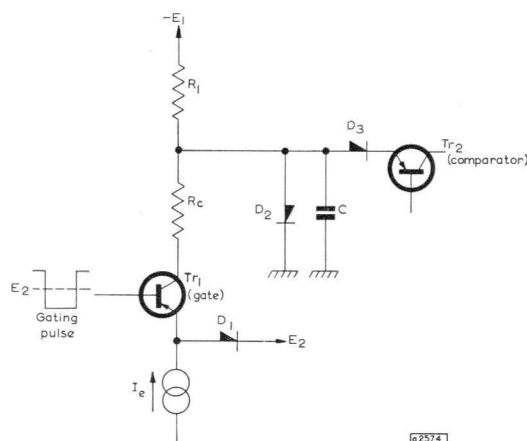


Fig. 19—Basic ramp generator

inductance, and also reduces the power dissipated in Tr_1 when E_2 is larger than the desired ramp amplitude. E_1 is a high-voltage negative supply rail (-250V in the circuits under consideration). An equivalent circuit is shown in Fig. 20 which includes all of the elements which might cause non-linearities in the generated ramp. There are two main effects which cause non-linearity. One is voltage dependent, and the other is time dependent; both are considered below.

Voltage-dependent Effect

A simplified equivalent circuit is shown in Fig. 21a. This shows only those components which significantly affect the shape of the charging curve at low frequencies. R_2 represents the parallel sum of $r_{cb'}$, R_{D2} and R_{D3} . This simplifies to Fig. 21b, where E_e is the effective 'aiming potential' and R is the effective charging resistor.

$$E_c = \text{steady state potential across } C \text{ with } I = I_e \text{ (that is, } i = 0) = I_e R_2 - \frac{I_e R_2 - E_1}{R_1 + R_2} R_2 = \frac{R_2}{R_1 + R_2} \cdot (I_e R_1 + E_1) \quad \dots(1)$$

$$\text{and } R = \frac{R_1 \cdot R_2}{R_1 + R_2} \quad \dots(2)$$

Thus, the charging current for small ramp amplitudes is $I_e - E_1/R_1$.

During the discharging period, $I = 0$, and the steady state

value of V is then E_D , where

$$E_D = E_1 \cdot \frac{R_2}{R_1 + R_2} \quad \dots (3)$$

Thus, the discharging current for small values of ramp voltages is $-E_1/R_1$ (Fig. 21c).

In practice, E_1 and I_e are fixed by other considerations. The ratio of discharging to charging-time, t_d/t_c (Fig. 21d), is

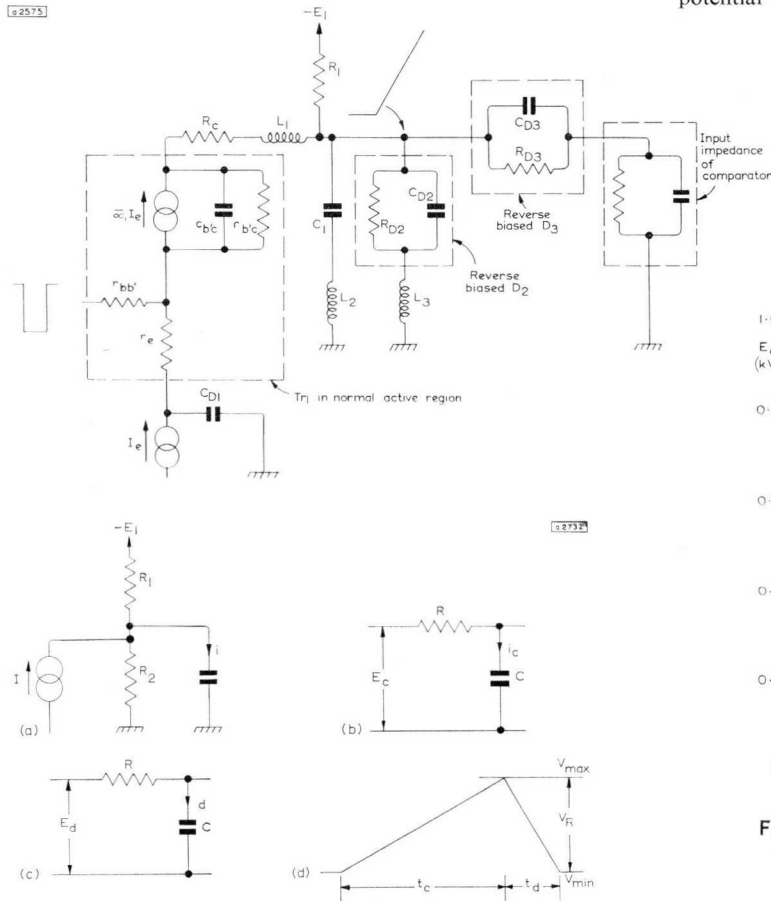


Fig. 21—Simplified circuit

also set by the available cycle-time. Let this ratio be called γ . These constants determine the value of R_1 .

We have

$$\gamma = \frac{t_d}{t_c} = \frac{i_c}{i_d} = \frac{E_c/R}{-E_D/R} = -\frac{E_c}{E_D}$$

Substituting for E_D from Eq(3)

$$\gamma = \frac{-E_c(R_1 + R_2)}{E_1 R_2} \quad \dots (4)$$

Substituting for E_c from Eq(1)

$$\gamma E_1 R_2 = \frac{-R_2}{R_1 + R_2} (I_e R_1 + E_1)(R_1 + R_2) \quad \dots (5)$$

whence

$$R_1 = \frac{(1 + \gamma)E_1}{I_e} \quad \dots (6)$$

From Eq(4)

$$E_c = \frac{\gamma E_1 R_2}{R_1 + R_2} = \frac{\gamma E_1 R_2}{E_1(1 + \gamma) - I_e R_2} \quad \dots (7)$$

This is the value of the aiming potential in terms of the initial constants, and shows that there is no optimum value for

I_e , but that E_c is asymptotic to $-\gamma E_1$ when $I_e \gg E_1(1 + \gamma)/R_2$.

Fig. 22 is a graph showing E_c versus I_e for $R_2 = 75k\Omega$ and $\gamma = 1, 2, 4, 7$ and 10 . (This value for R_2 is a minimum; values of up to $1M\Omega$ are typical when an ASZ21 transistor and AAZ13 diodes are used.) Note that when pulsed recharging is used (as in the circuits of Figs. 8 and 15b), the effective γ becomes very large since R_1 is high, and the aiming potential is very nearly $I_e R_2$. For $I_e = 10mA$ and $R_2 = 75k\Omega$ this potential is $750V$.

Fig. 20—Complete equivalent circuit of Fig. 19 during rise of ramp

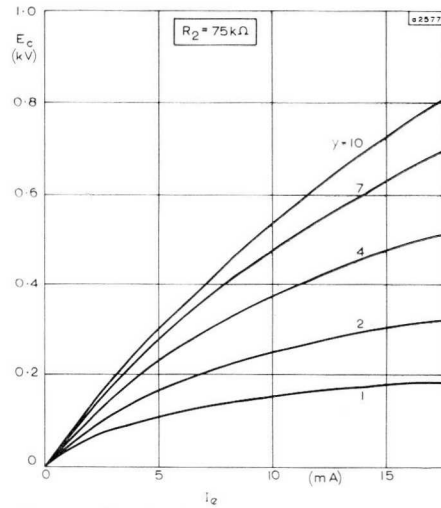


Fig. 22—Graph of effective charging potential

Non-linearity

The non-linearity error terms will be defined as

$$\delta_S = \frac{S_S - S_A}{S_A} \quad \dots (8)$$

and

$$\delta_F = \frac{S_F - S_A}{S_A} \quad \dots (9)$$

where

- δ_S = error at start of ramp
- δ_F = error at end of ramp
- S_S = initial slope
- S_F = final slope
- S_A = slope at half-amplitude.

Now,

$$S_S \propto E_c - V_{MIN}$$

$$S_F \propto E_c - V_{MAX}$$

$$S_A \propto E_c - \frac{V_{MIN} + V_{MAX}}{2}$$

Hence

$$\delta_S = \frac{E_c - V_{MIN} - E_c + \left(\frac{V_{MIN} + V_{MAX}}{2}\right)}{E_c - \left(\frac{V_{MIN} + V_{MAX}}{2}\right)} = \frac{V_R}{2E_c + V_R}$$

where

$$V_R = \text{ramp amplitude.}$$

Similarly,

$$\delta_F = \frac{-V_R}{2E_c + V_R}$$

Thus, the percentage non-linearity when $V_R \ll 2E_c$ is given by

$$\delta \approx \pm \frac{V_R}{2E_c} \times 100\% \quad \dots(10)$$

In a typical case, with $V_R = 5V$, and $E_c = 750V$, $\delta = \pm 0.3\%$.

Error Due to Voltage Sensitive Capacitances

The charging capacitance of Fig. 21 is made up as follows:

$$C = C_1 + C_{D2} + C_{D3} + C_{b'e} + \text{strays}$$

C_{D2} , C_{D3} and $C_{b'e}$ are dependent on their reverse bias voltage.

Let its value at the half-amplitude point be C ; at V_{MIN} let the value be $C + \Delta_1C$ and at V_{MAX} , $C + \Delta_2C$. (If D_2 and D_3 have very different capacitances, it is possible for Δ_1C or Δ_2C to be negative, but not both.)

For a constant charging current

$$\begin{aligned} S_A &\propto 1/C \\ S_S &\propto 1/(C + \Delta_1C) \\ S_F &\propto 1/(C + \Delta_2C) \end{aligned}$$

From Eq(8)

$$\delta_s = \frac{\left(\frac{1}{C + \Delta_1C}\right) - \left(\frac{1}{C}\right)}{(1/C)} = \frac{-\Delta_1C}{C + \Delta_1C}$$

Similarly

$$\delta_F = \frac{-\Delta_2C}{C + \Delta_2C}$$

When the characteristics of D_1 and D_2 are very similar, then $\Delta_1C \approx \Delta_2C$. (It is assumed that $C_{b'e}$ is approximately constant and small, since the collector of the driving transistor is always appreciably reverse-biased.) The percentage non-linearity is therefore

$$\delta = \frac{-\Delta C}{C + \Delta C} \times 100\% \quad \dots(11)$$

ΔC will always be substantially less than the capacitance of either diode at zero reverse bias, since C_{D2} decreases as V rises, especially at low values of delay bias. It is obvious that this effect is most severe on the fastest timebases, where C is small. For example, with $C = 50pF$ and $\Delta C = 2.5pF$ (the worst case)

$$\delta \approx \frac{2.5}{50} \times 100 = 5\%$$

Another component of the voltage-dependent effect occurs at the start of the ramp and is caused because D_2 does not fully become reverse-biased until the ramp has risen by 300 to 400mV, although the current in D_2 becomes negligible after a rise of about 100mV. This effect is avoided by setting the minimum pick-off voltage above this region, but at the expense of minimum delay.

Time-dependent Effects

Time-dependent effects result in non-linearity at the beginning of the ramp, and have a duration which is mainly independent of the range capacitor, and thus are more important on the fast ranges since the effects extend further into the main portion of the ramp.

The first effect is due to the finite switch-on time of Tr_1 (Fig. 19), which is about 3 to 5ns, and leads to a slow start. This effect is swamped by the delayed switch-off of D_2 mentioned above. A more important result of this fast step of current is caused by the stray inductance in series with the timing capacitor, L_2 and inductances L_1 and L_3 , in association with stray capacitances. This leads to ringing at the start of the ramp. Measurements show that a 5cm loop in this circuit typically introduces as much as half a volt of ringing at about 50Mc/s, and the only satisfactory solution is to keep the lead lengths to an absolute minimum. Carrier storage in D_2 also contributes to the non-linearity, but when the high-speed AAZ13 is used this effect is swamped by other effects.

Overall Linearity

The linearity of a complete delay system (Fig. 5) has been measured with a synchronised sinewave signal, and a null-detection method. Values of $< \pm 3\%$ for the '10ns' range and $< \pm 1.5\%$ for the '100ns' range between the 10% and 100% points were obtained. Errors over the first 10% of the ramp were somewhat greater, but could probably be improved by altering the circuit layout.

APPENDIX 3

Note on Waveforms

The waveforms which appear at the end of the article were made under the following conditions unless otherwise stated:
Oscilloscope: Tektronix 545A with CA plug-in and X10 P6000 probe or a type P6016 current probe.

Control settings on attachment:

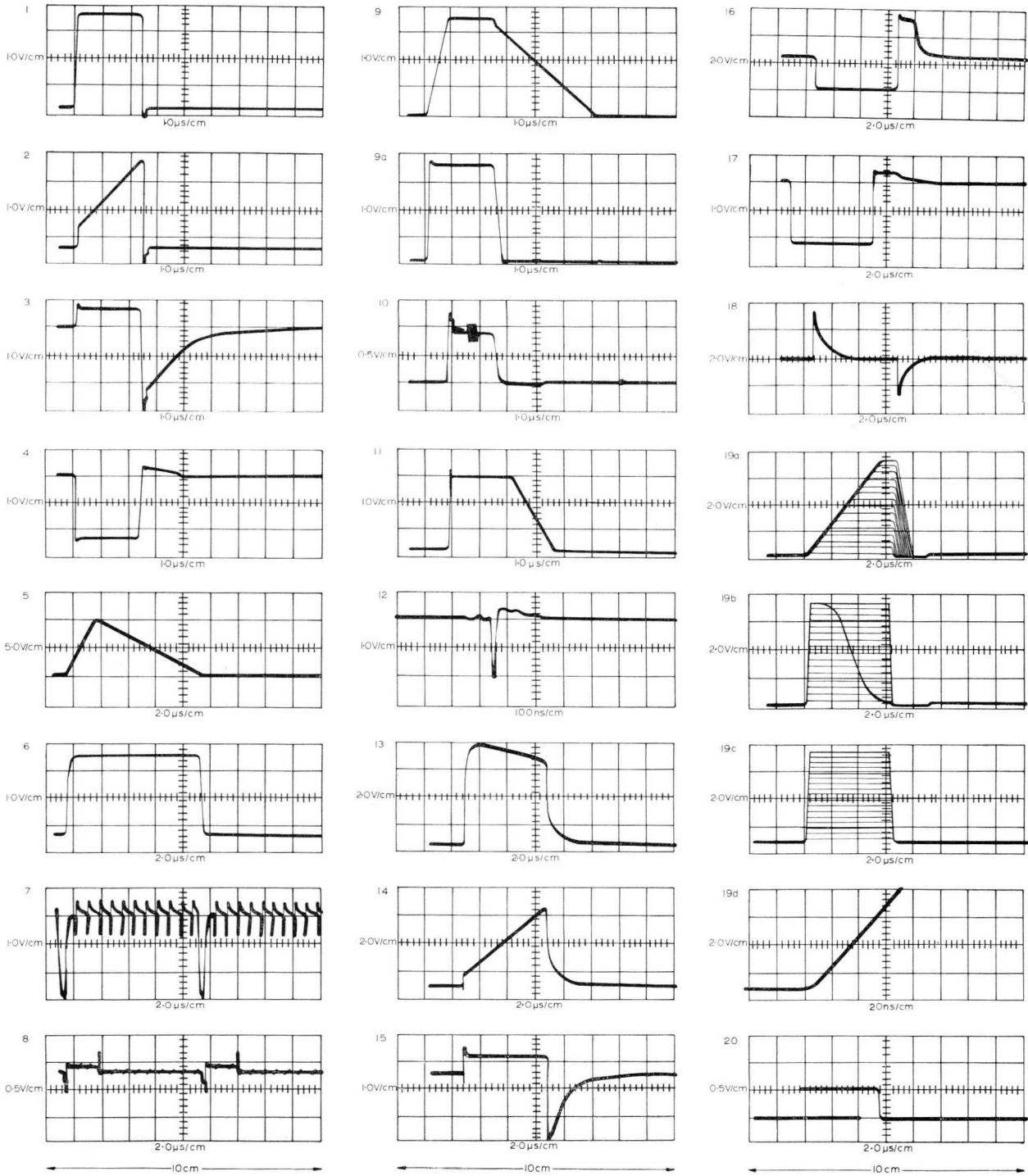
TIME/CM	: 0.5µs/cm
DOTS	: 150
DELAY	: 1µs
MULTIPLIER	: 0.8
DISPLAY LENGTH:	10cm

(All other controls set to give stable triggering)

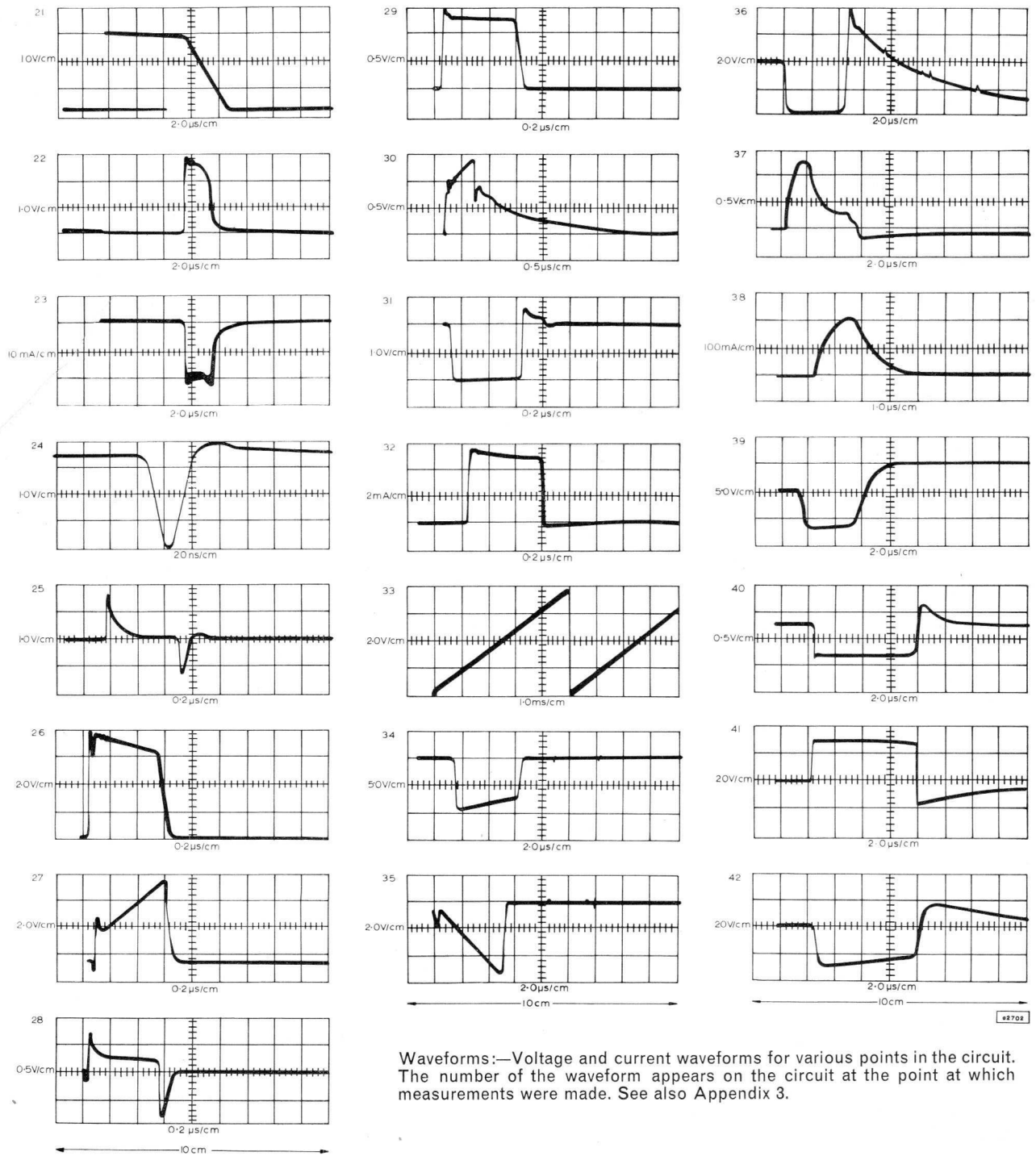
Trigger rate: 25kc/s

The waveforms are numbered 1 to 42. On the circuit diagrams, voltage waveforms and current waveforms are indicated, at the point at which measurements were made by a number corresponding to one of the numbered waveforms.

WAVEFORMS ARE SHOWN ON PAGES 225 AND 226.



TIMEBASES FOR SAMPLING OSCILLOSCOPES



Waveforms:—Voltage and current waveforms for various points in the circuit. The number of the waveform appears on the circuit at the point at which measurements were made. See also Appendix 3.

Microphony in Tape Recorders

S. S. DAGPUNAR

Mullard Applications Research Laboratory

Howback and clang microphony are the two most common types of interference experienced with a valve tape recorder. This article defines these terms and suggests design limits in the manufacture of valve tape recorders whereby these two types of microphony can be reduced to a satisfactory level.

INTRODUCTION

Microphony is occasionally experienced in a tape recorder where high gain a.f. valves are used in the first stages. There are two types of microphony: howback and clang microphony. The two types of interference are defined and discussed in detail under separate headings.

HOWBACK

Howback, or feedback howl, is an oscillation which occurs in the following way. Any excitation force may cause electrode vibrations in a valve resulting in an initial microphony (Ref. 1). The initial microphony of a pre-amplifier valve is then amplified and converted by the speaker into vibrations. These vibrations are fed to the valve acoustically, mechanically, or by a combination of both, in such a manner as to sustain the original electrode oscillations which produced the initial microphony.

Requirements

As implied in the definition of howback, this type of microphony occurs only if the valve is excited with a force of suitable phase and of sufficient amplitude. Therefore, even with a suitable phase relationship, howback will not occur if the equivalent microphonic grid voltage of the pre-amplifier valve (resulting from a specified speaker power) is less than the signal input voltage to the same valve required to produce the specified speaker power. This means that, for a speaker power of 1W and with a safety factor of two, the equivalent microphonic grid voltage $V_{eq(1W)}$ resulting from a speaker power of 1W, should be less than half the signal input voltage $V_{in(1W)}$ required for a speaker power of 1W. That is,

$$V_{eq(1W)} \leq \frac{1}{2} V_{in(1W)}$$

or, since $V_{eq(1W)} = V_{eq(1g)} g_{1W}$ and the speaker power is proportional to the square of the output or input voltage (or the input voltage is proportional to the square root of the speaker power),

$$V_{eq(1g)} g_{1W} \leq \frac{1}{2} V_{in(0.05W)} / \sqrt{0.05},$$

or

$$V_{eq(1g)} g_{1W} / V_{in(0.05W)} \leq 2.2 \quad \dots(1)$$

where

$V_{eq(1g)}$ = equivalent microphonic grid voltage of the pre-amplifier resulting from a peak acceleration of 1g,

g_{1W} = peak acceleration, in g, of the pre-amplifier valve resulting from a speaker power of 1W,

$V_{in(0.05W)}$ = signal input to the pre-amplifier valve required for a speaker power of 0.05W.

Design Limits

Valves which are intended for use in tape recorder input stages are designed with a $V_{eq(1g)}$ value such that they meet the requirement in Eq (1). This requirement applies in a tape recorder having a typical $g_{1W}/V_{in(0.05W)}$ ratio.

A typical ratio corresponds to the maximum possible values which occur in reasonably well-designed tape recorders. Normally, the valve published data give the recommended or minimum permissible value of $V_{in(0.05W)}$.

Maximum permissible average acceleration of the valve resulting from a speaker excitation of 50mW can be considered as 0.015g r.m.s. at frequencies higher than 500c/s, and 0.06g r.m.s. at frequencies lower than 500c/s. Considering that the maximum r.m.s. acceleration is equal to approximately three times the average r.m.s. acceleration (or $1/\sqrt{2}$ times the peak acceleration) and that the acceleration is proportional to the square root of the speaker power (Ref. 1), the maximum value of g_{1W} which should be used with the minimum $V_{in(0.05W)}$ is $3 \times 0.015 \sqrt{2} / \sqrt{0.05} = 0.28g$ for frequencies above 500c/s and $3 \times 0.06 \sqrt{2} / \sqrt{0.05} = 1.1g$ for frequencies lower than 500c/s.

Therefore, the maximum value of $g_{1W}/V_{in(0.05W)}$ is 0.28/recommended $V_{in(0.05W)}$ for frequencies above 500c/s and 1.1/recommended $V_{in(0.05W)}$ for frequencies lower than 500c/s. Consequently, howback microphony can reasonably be expected to result from the unsuitable design of the equipment if the $g_{1W}/V_{in(0.05W)}$ ratio is greater than the above-mentioned values.

CLANG

Clang is an audible interference caused by any external forces such as speaker, motors or especially switch excitations.

General Considerations

Clang may exist even at very low values of acceleration and low electrical sensitivities, although it is not necessarily objectionable at these levels. Thus, in an amplifier incorpo-

rating a speaker, if the gain is progressively increased, clang resulting from speaker excitation will be noticed first. Then, if the gain is further increased, up to a certain limit, howlback will occur.

In principle, the relative value of the interference with respect to the useful signal level determines whether the interference is negligible or not. With motor or switch excitation, the useful signal can be zero for a given interference. Therefore, ideally, the quality of motors, switches, and their mountings in the equipment should be such that the interference resulting from the excitation of these sources, with a useful signal level of zero, is not objectionable.

Generally, the clang resulting from switch excitation is more objectionable than that resulting from speaker or motor excitation. Therefore, switch excitation clang is discussed in detail and some practical requirements given.

Switch Excitation

It is important to distinguish between clang and mechanical interference. Clang is the electronic interference which is produced in the pre-amplifier valve and, after being amplified by the following stages, is audible from the loudspeaker. Mechanical interference is the sound of the switch operation as heard directly by the ear.

In the playback position the requirements for clang can be derived as follows. If the duration of the clang t_c is less than the duration of the mechanical interference t_m , the equivalent microphonic grid voltage $V_{eq(SW)}$, due to switch excitation, should be less than the signal input voltage $V_{in(P)}$ required for a speaker power of P watts, where P is the speaker output which has the same interference effect on the ear as that of the mechanical interference. That is,

$V_{eq(SW)} \leq V_{in(P)}$, or since $V_{eq(SW)} = V_{eq(1g)} g_{SW}$ and the input voltage is proportional to the square root of the speaker power,

$$V_{eq(1g)} g_{SW} \leq V_{in(0.05W)} \sqrt{\frac{P}{0.05}},$$

$$V_{eq(1g)} g_{SW} / V_{in(0.05W)} \sqrt{P} \leq 4.5 \quad \dots (2)$$

where g_{SW} = peak acceleration in g of the pre-amplifier valve resulting from the switching action.

If the duration of the clang is longer than that of the mechanical interference, experiment indicates that the ratio of the signal input voltage required for the maximum available speaker power $V_{in(P_o)max}$ to the equivalent microphonic grid voltage $V_{eq(SW)}$ should be greater than 24dB (16 times). That is,

$$V_{eq(SW)} / V_{in(P_o)max} < 1/16$$

or

$$\frac{V_{eq(1g)} \cdot g_{SW}}{V_{in(0.05W)} \sqrt{\frac{P_o max}{0.05}}} < 1/16$$

or

$$V_{eq(1g)} \cdot g_{SW} / V_{in(0.05W)} \sqrt{P_o(max)} < 0.3 \quad \dots (3)$$

Poor mechanical design of the equipment can produce a ringing effect and make the duration of the clang longer than that of the mechanical interference. Therefore, the problem of ringing effects should be taken into account at the design stage of the tape recorder. Thus the duration of clang would not exceed the duration of the mechanical

interference and consequently, the rather rigid requirements of Eq (3) need not be considered.

Design limits for clang microphony can be derived simply, as discussed in the results given for howlback by using Eq (2) and (3) with the following typical values.

PERFORMANCE OF THREE TYPICAL TAPE RECORDERS

Measurements have been made on three different types of commercially available tape recorder.

Vibration

The acceleration of the pre-amplifier valve resulting from a speaker power of 50mW was measured, in three mutually perpendicular directions, by a Brüel and Kjaer accelerameter, type 4329, mounted on the valve socket. The peak accelerations caused by a 0.05W speaker power in the frequency spectra above 500 and below 500c/s were less than 0.05 and 0.15g respectively. The peak accelerations g_{1W} corresponding to a speaker power of 1W in the same frequency spectra were less than 0.2 and 0.7g respectively. The peak-to-peak acceleration (that is $2g_{SW}$) resulting from the operation of switches was between 0.5 and 2g, with durations of 15 to 60ms and frequencies up to 500c/s.

Electrical Sensitivity

In the playback position, the value of the input voltage $V_{in(0.05W)}$, in the frequency range 50 to 10 000c/s, varied with frequency and the individual equipment from 0.1 to 0.8mV. The maximum available speaker power $P_o(max)$ varied between 1 and 3W.

Howlback, Clang and Mechanical Interference

Howlback and clang tests were carried out on the playback position with the volume control at maximum. No interference could be detected by ear.

Mechanical interference and clang resulting from switch operations were measured with a Peekel Sound Spectrometer, type GR3, and an oscilloscope. The two sources of interference were isolated with a sound-proof box, and the following results obtained:

Duration of mechanical interference $t_m = 50$ to 200ms.

Duration of clang $t_c = 20$ to 30ms.

The relative amplitude of clang with respect to the amplitude of the mechanical interference, as sensed by the spectrometer = 0.2 to 0.7.

The speaker power required to produce the same interference effect on the spectrometer as that of the mechanical interference of the switching action = 0.9 to 2.5W.

Thus, in the three tape recorders examined, it was found that clang and howlback microphony were within the limits given in this article.

REFERENCES

1. DAGPUNAR, S. S. 'Valve Microphony'. *Mullard Technical Communications*, Vol. 7, No. 61, Nov. 1962, pp. 2 to 17.



MULLARD LIMITED

Mullard House

Torrington Place

London, W.C.1

CONTENTS

Transistor Decoder Circuits for F.M. Stereo Broadcasting	202-205
Capacitive Intermodulation in Dual-trace Oscilloscope Tubes	206-210
Timebases for Sampling Oscilloscopes	211-226
Microphony in Tape Recorders	227-228

VOL. 7 No. 67 DECEMBER 1963

